Hydrocarbon Oxidation Products in Cook Inlet: Formation and Bioaccumulation in Mussels

Principal Investigators: Patrick L. Tomco[1] David C. Podgorski[2], Phoebe A. Zito[2], Zachary C. Redman[1]

[1] University of Alaska Anchorage, Department of Chemistry

[2] University of New Orleans, Department of Chemistry

December 2023
Final Report
OCS Study BOEM 2023-028

Contact Information:
uaf-cmi@alaska.edu
https://www.uaf.edu/cfos/research/cmi

This study was funded by the University of Alaska Coastal Marine Institute and the U.S. Department of the Interior, Bureau of Ocean Energy Management Alaska OCS Region (cooperative agreement M20AC10012). This report, OCS Study BOEM 2023-028, is available electronically from https://www.boem.gov/akpubs

Citation:

P.L Tomco, D.C. Podgorski, P.A. Zito, Z.C. Redman. 2023. Hydrocarbon oxidation products in Cook Inlet: formation and bioaccumulation in mussels. Fairbanks (AK): University of Alaska Coastal Marine Institute and U.S. Department of the Interior, Bureau of Ocean Energy Management, Alaska OCS Region. 55 p. Report No.: OCS Study BOEM 2023-028. Contract No.: M20AC10012.

TABLE OF CONTENTS

LIST OF FIGURES iii
LIST OF ACRONYMS iv
ABSTRACT 1
INTRODUCTION 2
Background 2
Objectives and Hypotheses 5
METHODS 6
Laboratory Simulated Oil Spill 6
Dissolved Organic Carbon (DOC) Analysis 6
Excitation-Emission Matrix Spectroscopy (EEMs) 7
LC-Orbitrap mass spectrometry 7
Targeted analysis of OxyPAHs and PAHs 8
Mussel Exposure to HOPs 8
Analysis of oxyPAHs in Mussels 9
RESULTS AND DISCUSSION 10
Photoproduction of HOPs 10
Optical Characterization of HOPs 10
Molecular Characterization of HOPs 13
Detection of OxyPAHs and PAHs in HOPs 17
Bioaccumulation of OxyPAHs in Mussels 18
CONCLUSIONS 19
ACKNOWLEDGMENTS 20
STUDY PRODUCTS 20
Publications 20
Presentations 20
REFERENCES 22
APPENDICES 33

List of Figures

Figure 1. Pathways for the photo-enhancement of crude oil toxicity by (a) in-vivo photosensitization and (b) ex-vivo photo-modification of polycyclic aromatic hydrocarbons (PAHs). Mussels have shells that shield UV light; therefore pathway (b) is most relevant to this organism.

Figure 2. Temporal shifts in DOC for HOPs in all samples.

Figure 3. (a) PARAFAC components (b) PCA biplot, loadings represent PARAFAC components. (c) Temporal relationship between C3 and C4 in HOPs formed from light irradiated diesel.

Figure 4. Heteroatom oxygen class graphs from day 10 samples, CI crude oil (red), diesel (blue), irradiated (top), dark (bottom).

Figure 5. van Krevelen subtraction plots of day 10 dark and light treatments for CI crude oil and diesel where each data point represents a unique molecular feature. Photochemical processing of CI crude oil has 2484 unique features and diesel has 2293 unique features.

Figure 6. PCA biplot, loadings represent molecular classifications.

Figure 7. (a) OxyPAHs and their respective PAH derivatives and (b) methylated naphthalene concentrations in HOPs formed from irradiated CI Crude oil.

Figure 8. Mussel tissue analyses of oxyPAHs. (a) Detection of 9-fluorenone by LC-Orbitrap confirms good spike recovery of 9-fluorenone with trace detection in samples and method blank. Unfortunately, detections in mussels exposed to HOPs could not be distinguished from background seawater controls. (b) Product ion spectrum for 9-fluorenone positively confirms compound identity based on the characteristic fragmentation of the precursor ion (181.0650 *m/z*).

List of Acronyms

AImod:	Modified Aromaticity Index
ANOVA:	Analysis of Variance
BOEM:	Bureau of Ocean Energy Management
BTEX:	Benzene, Toluene, Ethylbenzene, and Xylene
CA:	Condensed Aromatic
CI:	Cook Inlet
DOC:	Dissolved Organic Carbon
EEMs:	Excitation - Emission Matrices
EIS:	Environmental Impact Statement
GC-MS:	Gas Chromatography Mass Spectrometry
HIX:	Humification Index
HOPs:	Hydrocarbon Oxidation Products
LC-QQQ:	Liquid chromatography triple quadrupole
LC:	Liquid Chromatography
NAs:	Naphthenic Acids
OWM:	Oil Weathering Model
oxyPAHs:	Oxidized Polycyclic Aromatic Hydrocarbons
PAHs:	Polycyclic Aromatic Hydrocarbons
PARAFAC:	Parallel Factorial Analysis
PCA:	Principle Component Analysis
SPE:	Solid Phase Extraction
SUVA254:	Specific UV Absorbance at 254 nm
TPH:	Total Petroleum Hydrocarbons
UHO:	Unsaturated High Oxygenation
UHPLC:	Ultra-high pressure liquid chromatography
UHR-MS:	Ultra-high resolution mass spectrometry
ULO:	Unsaturated Low Oxygenation

ABSTRACT

This study was conducted to map the chemical properties of hydrocarbon oxidation products (HOPs) that could form under the environmental conditions of Cook Inlet (CI) within south-central Alaska from CI crude oil and diesel feedstocks exposed to sunlight over a 10-day period. Two sets of analyses were performed to identify and characterize the HOPs. The first set of analyses performed was non-targeted and included high-resolution mass spectrometry and fluorescence excitation-emission matrix spectroscopy. Liquid chromatography coupled with an Orbitrap mass spectrometer uncovered that HOPs formed from CI crude oil and diesel are relatively reduced, saturated, and unsaturated compounds. The molecular composition of HOPs from crude oil are more aromatic, whereas those formed from diesel are more aliphatic. Six unique chemical features of HOPs were revealed by fluorescence excitation-emission matrix spectroscopy, including two unique petroleum signatures. The parallel factor model for fluorescence excitation-emission matrix spectroscopy accurately tracks temporal compositional changes of HOPs. The second set of analyses was targeted and included the quantification of polycyclic aromatic hydrocarbons (PAHs) and oxygenated polycyclic aromatic hydrocarbons (oxyPAHs) in HOPs using tandem mass spectrometry. Two oxyPAHs, phenanthrenequinone, and 1,4-anthraquinone, were quantified in HOPs formed from CI crude oil and related to eleven PAHs. No oxyPAHs were detected in mussel tissues, which we believe indicates that targeted analytical approaches are not environmentally relevant for classifying HOPs. Instead, non-targeted approaches have the potential to be much more successful in describing this class of compounds. The results from this study uncover a comprehensive approach to monitoring compositional changes of hydrocarbon oxidation products in a crude oil or diesel spill event.

INTRODUCTION

Background.

Response to oil spills at high latitudes is challenging due to complicated mechanical oil recovery techniques in icy environments. With the increase in petroleum development, presence of infrastructure to hold and deliver petroleum, and the problematic nature of responding to high latitude spill events, it is imperative to understand the characteristics, transport, and fate, of spilled oil in the Arctic and subarctic environments.[1]

Hydrocarbon oxidation products (HOPs) are formed in the environment by weathering of spilled oil. HOPs are dissolved oxidized petroleum products that have not fully degraded into seawater. Crude oil and diesel fuel are complex mixtures of naturally occurring organic matter predominantly composed of hydrocarbons, with minor contributions from nitrogen, sulfur, oxygen, and trace metals. Once spilled into the marine environment, oxygenation by photochemical and microbial processes result in the formation of HOPs[2]. Photochemical degradation processes produce HOPs in oxic environments by reacting with aromatic compounds that absorb light in the solar spectrum; microbes can also produce HOPs through both aerobic and anaerobic biotransformation processes[3-6]. Both of these pathways result in the production of an entire range of highly water-soluble bioavailable compounds, including both parent and "dead-end" oxidation products[7-9]. HOPs may be distributed throughout aquatic environments once it is mobilized as a result of dissolution, impacting coastal ecosystems.

HOPs are more bioavailable in the marine environment than their parent petroleum molecules and must be detected accurately to assess the extent of petroleum-derived contaminants. Aquatic ecosystems are particularly susceptible to contamination from HOPs that can be readily transported through water movement (e.g., in fluvial networks, ocean currents, between groundwater and surface waters)[10-12]. Tracking the migration, concentration, chemical composition, and potential toxicity of these complex mixtures is critical for making both short- and long-term spill-response decisions. Post spill, long-term observations are required to determine the fate of the contaminants and degradation products in the surrounding marine environment[13]. Although detection, response, and cleanup efforts focus on the visible and water accommodated fractions of petroleum, the dissolved fraction of oxygenated weathered products are more mobile in aquatic ecosystems[14]. The high solubility of HOPs enables it to rapidly diffuse both vertically and laterally in a water column, which means these compounds can travel undetected vast distances ahead of any signs of a visible oil front, particularly in the case of a surface spill.

HOPs and their petroleum parent compounds are challenging to characterize with traditional mass spectrometry techniques because the chemical composition of oil is complex, with over 100,000 identified molecular formulae, and they reside in the unresolved complex mixture.[20-22] Recent studies employed various complementary analytical techniques, such as gas chromatography-mass spectrometry (GC-MS), ultrahigh-resolution mass spectrometry (UHR-

MS), etc., to address this knowledge gap [20, 23-29]. This study utilizes complementary non-targeted and targeted techniques. Non-targeted analyses include two complementary analytical methods, LC-Orbitrap, to characterize the molecular-level composition and fluorescence excitation-emission matrix spectroscopy (EEMs) to characterize the optical properties of HOPs. The non-targeted techniques employed, LC-Orbitrap and EEMs, utilize similar fingerprinting type analyses that produce data, without a-priori knowledge, that is further reduced into chemical categories grouped by compositional similarities. The targeted analysis includes liquid chromatography – triple quadrupole mass spectrometry (LC-QQQ) to quantify a suite of commercially available oxyPAHs in HOPs generated from CI crude oil and diesel.[30] OxyPAHs are more water soluble and thus are potentially more bioavailable than PAHs.[31,32] Some studies indicate the class of oxyPAH compounds are more toxic in the environment[33-35].

It is important to monitor HOPs because photo-enhanced toxicity of crude oil is a real possibility. In both ice-associated and open water conditions, whenever oil is exposed to the surface, the presence of sunlight may be a confounding variable affecting the weathering of oil and our understanding of spilled oil toxicology[39]. Exposure to sunlight adds oxygen to crude oil, changing the oil's chemical and physical properties and allowing the oxygenated hydrocarbons to dissolve in water. Photo-enhanced toxicity, (i.e. the increase in toxicity associated with the presence of sunlight), of oil has been identified in many studies over the past 20 years to various marine species, including copepods[40], eastern oyster larvae[41], crab larvae[40,42], mysid shrimp, and various fish[43,44]. Pelletier et al. (1997)[45] determined that light enhanced the toxicity of crude oil 2–100 fold and the toxicity of anthracene, fluoranthene and pyrene (chemical compounds in oil) 12–50,000 fold. There are two pathways of photo-enhanced toxicity (**Figure 1**): photosensitization (initial hydrocarbon bioaccumulation, followed by UV activation of residues in translucent tissue) and photomodification (exposure to the oxidized hydrocarbons formed upon exposure of oil to sunlight)[46]. Given that the shells of mussels act as a shield for UV exposure, we anticipate that photomodification is most relevant to observed toxicological endpoints. This pathway has been documented previously in juvenile bivalves[47]. An oil spill in Cook Inlet regions during the summer would expose oil to sunlight for 16 hours per day and may result in significant photo-enhanced toxicity. Photo-enhanced toxicity can be a factor in the decision to deploy oil spill response chemicals, e.g., dispersants, conduct *in-situ* burning, deploy surface cleaning agents, collect oil with chemical herder prior to *in-situ* burning, etc. The "decision-tree" strategy for the "appropriate" response requires careful consideration of the process whereby oil is transformed into a water-soluble (more bioavailable) state. Prior studies have focused on chemical changes that accompany photo-modified oil, toxicological effects in mussels, but there is a lack of basic understanding of the bioaccumulation potential and baseline presence of oxidized residues in mussel tissues, which may be generated through either photo-sensitized or photo-modified means. This need has been established in the Gulf of Mexico region following the Deepwater Horizon Oil Spill[48], and with new advances in the capacities of Mass Spectrometry and spectrofluorimetry to

profile oxidized hydrocarbons, our project addresses the BOEM-relevant needs to understand these effects and enable future efforts on fate, transport, and monitoring.

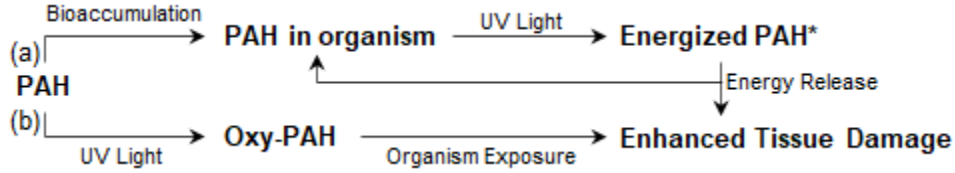

Figure 1. Pathways for the photo-enhancement of crude oil toxicity by (a) in-vivo photosensitization and (b) ex-vivo photo-modification of polycyclic aromatic hydrocarbons (PAHs). Mussels have shells that shield UV light; therefore pathway (b) is most relevant to this organism.

PAHs have been the focus of past research because this class of compounds could be easily analyzed using the prevailing technology available at the time. Since the Deepwater Horizon event, new technologies have opened the analytical window to HOPs and established the significance of HOPs. Thus, there is a need to establish a baseline monitoring of HOPs in Cook Inlet. This is needed to assist in future tracking of a potential spill in the region and to determine their ultimate fate in the environment. Recent studies have demonstrated the bioaccumulation and toxicological importance of this chemical compound class[15-18]; however, no baseline information exists for Cook Inlet. Existing research is difficult to apply to Cook Inlet because it was often conducted in regions of warmer temperatures and/or on different oil types. For instance, polycyclic aromatic hydrocarbon levels have been extensively monitored, however little/no information in this region exists on baseline levels of their transformation products, oxygenated polyaromatic hydrocarbons (oxyPAHs). This project aims to identify HOPs, which includes oxyPAHs[19], formed by crude oil and diesel fuel in simulated bench-scale spills, perform correlations to broad molecular characterization, and identify potential uptake in marine organisms.

Cook Inlet is a crucial watershed in Southcentral Alaska due to the major population centers surrounding it, commercial fishing, subsistence, tourism, and the diverse wildlife it supports. In addition, the region is an oil-producing basin with new lease sales and developments.[1] The Environmental Impact Statement (EIS) of Cook Inlet oil and gas lease sale uses an Oil Weathering Model (OWM) that assumes a crude oil or diesel spill would be 1,700–5,100 bbls, occur at the surface or near-surface, over a short period, and persist up to 30 days.[1] The OWM conditions allow spilled oil to be weathered into HOPs, which is acknowledged in the EIS, but no fate/transport models include this class of compounds. The routine analysis of petroleum compounds in Cook Inlet as aromatic hydrocarbons (benzene, toluene, ethylbenzene, and xylene (BTEX); polycyclic aromatic hydrocarbons (PAHs); and total petroleum hydrocarbons (TPH)) has occurred for the past 40 years.[1] Currently, there are no routine monitoring of HOPs in Cook Inlet. The techniques outlined in this study can supplement existing analyses to more accurately understand the effects

of an oil spill in Cook Inlet. This will help promote the Bureau of Ocean Energy Management (BOEM) mission to promote environmentally safe development of petroleum resources in Cook Inlet. This research helps identify the molecular composition of this chemical class that *could* result from spilled crude oil or diesel fuel in Cook Inlet, and identify whether ambient levels exist in simulated seawater, and mussel tissues across the region. This data would assist BOEM in evaluating the fate and transport of a hypothetical spill for environmental impact assessment.

Blue mussels are well-established biomonitors for toxicity assessments. This project focuses on connecting the weathering patterns of spilled oil to the bioaccumulation of oxidized and fresh petroleum-derived residues using blue mussels (*Mytilus trossulus)* as a sentinel species. *Mytilus trossulus* are ubiquitous, sessile organisms that bioaccumulate pollutants through filter-feeding. They are an integral component of coastal ecosystems and an important food source for both wildlife and humans[36]. Blue mussels are easily sampled for cost-effective monitoring programs in the case of an oil spill. Therefore, we selected *Mytilus trossulus* for use in this project because it is a cold-water species of commercial, subsistence and ecological importance in both the Arctic and subarctic. Mussels are ubiquitous invertebrates in the intertidal zone of Cook Inlet and are important prey for a variety of organisms including snails, sea stars, octopus, crabs, seabirds, sea ducks and sea otters[37]. In addition to adult mussels serving as a primary food resource for many species, mussel larvae are an important component of plankton, contributing up to 50% of total zooplankton during peak spawning season, an important food resource for larval fish, filter feeders and other zooplankton[38]. Mussels also clear the water through continuous filter feeding and can accumulate contaminants such as crude oil. *Mytilus trossulus* is found from the Arctic south along the Alaskan coast to northern California and in the northern Atlantic. Mussels are lipid rich, indicating a possibility for bioaccumulation of toxicants such as HOPs and biomagnification at higher trophic levels. Additionally, spawning may be a mechanism for the organism to reduce its contaminant burden, as the majority of lipids are in the gonads. These factors all indicate *Mytilus trossulus* is an appropriate model organism for this region and class of contaminants.

Objectives and Hypotheses.

The goal of this project is to identify HOPs that are produced when CI crude oil and diesel are discharged into Cook Inlet. The results from the successful completion of the project provide new insights into the transformations of hydrocarbons in seawater and a superficial assessment of the levels of these compounds in mussels. Information about the concentration and chemical composition of the HOPs will lead to better treatment and monitoring strategies. Information on HOP bioaccumulation can inform future toxicological studies such as the assessment of sublethal stress. Also, fluorescence data is useful to both characterize HOPs and inform the development of new sensors for future baseline monitoring of these products in Cook Inlet, e.g., those that can be deployed on weather buoys and monitored in real-time over cellular or satellite data networks. The

use of a combination of analytical techniques enables us to distinguish signatures and/or classify compounds to account for contributions from hydrocarbons and HOPs.

This study is organized around three Objectives to accomplish the overall goal. Objective 1 is to simulate leaks and spills of crude oil and diesel with Cook Inlet seawater; Objective 2 is to identify the production of HOPs in laboratory simulations; and Objective 3 is to identify bioaccumulation of HOPs in Cook Inlet mussels in laboratory simulations. We *hypothesize* that HOPs can be detected in Cook Inlet seawater when incubated with oil and exposed to sunlight; and we *hypothesize* that HOPs bioaccumulate in mussel tissues when exposed to sunlight-exposed oiled seawater

METHODS

Laboratory Simulated Oil Spill.

Laboratory simulated oil spills of CI crude oil (provided by Blue Crest Energy) and diesel (obtained by Shoreside Petroleum) were performed using a solar simulator (Atlas Suntest XLS+). Diurnal seawater temperature (12 °C) and sunlight exposure (250 W/m^2) of Cook Inlet in the summer (June–August) was used.[49] Each oil substrate was added to artificial seawater (made with Instant Ocean Sea Salt at 36.86 g/L in Milli-Q water (18.2 MΩ cm)) at an oil load of 63.8 µl per 50 mL water in 100 mL thermostatically controlled jacketed beaker, consistent with prior studies that aim to create ~100 µm film thickness. Artificial seawater was used in this study to avoid background interference from dissolved organic matter or reactions from natural water. The composition of Instant Ocean Sea Salt has been previously reported and accurately represents the ionic strength of natural seawater.[50] Each jacketed beaker represents a single time point (irradiation period). There were four time points in the experiment, 1, 4, 7, and 10 days. Each time point for each oil substrate was analyzed in triplicate. Quartz lids were used to cover each beaker to reduce evaporation. An additional set of samples were incubated in the dark as a control to address any concerns of oxidation due to non-photolytic processes. Day 10 dark control samples for CI crude oil and diesel were completed on a larger scale of an oil load of 12.78 mL per 1000 mL of water to ensure enough control substrate was produced for ultrahigh resolution mass spectrometry. After each exposure, water and oil were separated and filtered through a 0.27 µm glass fiber filter pre-combusted at 550 °C and stored at -20 °C until analysis.

Dissolved Organic Carbon (DOC) Analysis.

Each sample was filtered through a pre-combusted (550 °C > 4 hours) Advantec GF-75 0.3 µm glass fiber filter into a pre-combusted amber glass vial. The pH of each sample was adjusted with high-purity hydrochloric acid to pH < 2. Samples were stored in the dark and refrigerated (< 4 °C) until they were ready for analysis. Samples were analyzed for DOC concentration with a Shimadzu TOC-V system equipped with an autosampler. DOC was measured as non-purgeable

organic carbon converted to CO_2 and detected by a non-dispersive infrared detector.[51] DOC was calibrated with potassium hydrogen phthalate, and DOC standards were run regularly.

Excitation-Emission Matrix Spectroscopy (EEMs).

The pH of filtered samples was adjusted to pH 8 with NaOH for absorbance and fluorescence measurements with an Aqualog® fluorometer (Horiba Scientific, Kyoto, Japan).[52-54] Optical measurements were carried out in a 10 mm quartz cuvette, an excitation range from 240–800 nm in 5 nm increments, and an emission range from 240–828.16 nm in 2.34 nm increments with an integration period of 1.5 s for light-exposed samples and 15 s for dark control samples. Each sample was diluted to an absorbance of 0.1 at 254 nm to reduce inner filter effects, using Milli-Q water (18.2 MΩ cm) to dilute.[55,56] Spectra were blank subtracted and corrected for instrument bias in excitation and emission prior to correction for inner filter effects. Fluorescence intensities were normalized to Raman scattering units, and dilution was corrected prior to PARAFAC analysis. The drEEM toolbox and MATLAB code were utilized to complete PARAFAC of the EEMs.[57] The spectral properties of the resulting statistical model were validated by residual and split-half analysis.[58,59] The validated model was uploaded to the OpenFluor database to compare with published models above 95% similarity score.[60]

LC-Orbitrap mass spectrometry.

The filtrate from light-exposed samples on days 4, 7, and 10 and dark control day 10 for CI crude oil and diesel were acidified to pH 2 and extracted via solid phase extraction (SPE) with Varian Bond Elut PPL cartridges (1 g, 6 mL).[61] SPE is an efficient method for isolating high-purity dissolved organic carbon extracts from the water-soluble fraction of oil.[62] The final concentrations of the extracts were adjusted to 500 μgC mL^{-1} to normalize carbon loads across samples to uncover compositional trends and stored at -20 °C before analysis.[61] Due to low DOC values and limited sample amount in the dark samples, only day 10 of dark CI crude oil and diesel underwent LC-Orbitrap analysis.

Collected mass spectra were co-added across the chromatogram, internally recalibrated with a "walking" calibration equation, followed by a blank subtraction and molecular formula assignment (C4-50, H4-100, O1-40, N0-2, S0-1) with Composer software (Sierra Analytics). Molecular formula assignment constraints were based on Hawkes et al. (2020), including double bond equivalents minus oxygen ≤ 10, O/C ≤ 1.2, 0.3 ≤ H/C ≤ 2.2, and Kendrick mass defect ≤ 0.4 or ≥ 0.9.[63] Molecular formulae were classified based on stoichiometry into the following categories: condensed aromatic (CA) (modified aromaticity index (AI_{mod}) ≥ 0.67), aromatic (0.67 > AI_{mod} ≥ 0.5), unsaturated low oxygen (ULO) (AI_{mod} < 0.5, H/C < 1.5, O/C < 0.5), unsaturated high oxygen (UHO) (AI_{mod} < 0.5, H/C < 1.5, O/C ≥ 0.5), aliphatic (H/C ≥ 1.5), and classically defined naphthenic acids ($C_nH_{2n+z}O_2$ in which n is the number of carbon atoms and Z is zero or a negative even number that represent hydrogen deficiency, and exclusion rules

reported by Holowenko et al. (2002) to eliminate carbon number groups and Z family values that do not conform to the empirical formula).[64-68]

Targeted analysis of OxyPAHs and PAHs.

Eight oxyPAHs and 24 PAHs were chosen for the targeted analysis of oxyPAHs and PAHs in HOPs formed from CI crude oil and diesel. The oxyPAH compounds were, 1-naphthol, 2-naphthol, phenanthrenequinone, 1,4-anthraquinone, 1-hydroxy-9,10-anthraquinone, 1,4-chrysenequinone, 5,12-naphthacenequinone and benzanthraquinone. The PAH compounds were naphthalene, acenaphthylene, 1-methylnaphthalene, 2-methylnaphthalene, acenaphthene, fluorene, 9-methyl-9H-fluorene, phenanthrene, 2,6-dimethylnaphthalene, anthracene, fluoranthene, 2,3,6-trimethylnaphthalene, 9-methylanthracene, pyrene, 9,10-dimethylanthracene, 1-methylpyrene, benz(a)anthracene, chrysene, benzo(a)pyrene, benzo(b)fluoranthene, benzo(k)fluoranthene, benzo(ghi)perylene, dibenzo(ah)anthracene, and indenopyrene.

The aqueous filtrate of the dissolved phase from CI crude oil and diesel experiments was added into different separatory funnels, and deuterated PAH surrogates (Table A10) were added to the filtrate to make a 1 µg/L concentration. Liquid-liquid extraction was performed three times with 20 mL of 9:1 chloroform:tetrahydrofuran as a solvent and anhydrous Na_2SO_4 as a drying agent for the organic layer. A liquid-liquid extraction procedure was optimized as extraction recoveries using dispersive liquid-liquid micro extractions reported in the literature were not reproducible.[69] During optimization, chloroform yielded higher extraction recoveries for both PAHs and oxyPAHs when compared to ethyl acetate and dichloromethane; further addition of tetrahydrofuran as a dispersive solvent to increase chloroform-artificial seawater biphase interaction improved oxyPAH extraction efficiency. Approximately 60 mL of the organic extract was evaporated to 0.1 mL under N_2 at 25 °C. 5 µl of 10 µg/mL deuterated PAH internal standard solution was added. Each extract was then reconstituted in 10 mL of methanol before being evaporated to 1 mL. Finally, the extracts were filtered through a 0.2 µm nylon filter and stored at -20 °C until analysis. Average recoveries (n = 6) were 69.3 ± 13.6 - 88.4 ± 15.2 % and 89.7 ± 6.9 - 125.4 ± 26.0 % for oxyPAHs and PAHs, respectively, with the exception of anthraquinone (24.8 ± 7.7 %) and 1,4-chrysenequinone (5.8 ± 1.8 %) which were ineffectively recovered by this method (Table A6). To our knowledge, no previous studies report higher recoveries for oxyPAHs.[70]

Mussel Exposure to HOPs.

In the fall of 2021, collaborators from the Cook Inlet Regional Citizens Advisory Council collected 326 blue mussels (*Mytilus trossulus*) from Kachemak Bay, near Seldovia, AK. The mussels were transported to the Alaska SeaLife Center in Seward, AK, where they were acclimated before undergoing a controlled exposure at 12 °C to (1) clean seawater, (2) seawater with diesel hydrocarbon oxidation products, or (3) seawater with Cook Inlet crude oil hydrocarbon oxidation products. Mortality checks and measurements for pH, dissolved oxygen content, and temperature were taken daily. Mussels were collected in triplicate after 24, 48, and

96 hr of exposure. Twenty-seven mussels from each exposure type were collected at each time point, allowing for 3 mussels in each exposure type to be subjected to a 96-hour recovery period in clean seawater. However, at the 24-hour time point, 30 mussels from the diesel exposures had expired, at which point their tissue was removed from the shell and stored for later analysis. While this petroleum load was identical to crude oil (volume equivalency basis), the mortality rates of diesel were surprisingly high. At 48 hours, an additional 10 mussels from the diesel exposure were found deceased, and their soft tissue was collected. Due to the exceedingly high mortality rate in the diesel exposures, those remaining, living mussels from the diesel exposure began their 96-hour recovery period after 48 hours instead of 96 hours; all mussels from the diesel exposure containers survived the 96-hour recovery period in clean seawater. There were no mortalities observed in the clean seawater containers, and only one mortality was observed in the containers with seawater and crude oil from 96 hr exposure. Mussels were collected and stored individually after measurements of sex, shell length, height, width, total weight and empty shell weight were recorded. The tissue was stored at -80℃ until extraction.

Analysis of oxyPAHs in Mussels.

Mussels were extracted according to protocols developed by DeWitte et al. (2019)[30] Briefly, mussels from each treatment and timepoint were homogenized and 3 g of tissue was extracted via pressurized liquid extraction using an ASE 200 (Dionex). Mussel tissues were spiked with 5 µL of 10 µg/mL solution of the surrogate standard 1-pyrenecarboxaldehyde prior to filling extraction cells with sodium sulfate and diatomaceous earth. Each sample was extracted in three cycles (5 min, 100 °C) with hexane:acetone (3:1, v/v). Extracts were reduced to 1.0 mL under N_2 prior to solid phase extraction (SPE) cleanup with silica gel. Cleaned extracts (hexane:isopropanol, 90:10, v/v) were solvent exchanged into methanol and reduced to 1.0 mL under N_2 prior to LC-Orbitrap targeted analysis. The targeted analysis of oxyPAHs was migrated to LC-Orbitrap from LC-QQQ to incorporate the surrogate standard 1-pyrenecarboxaldehyde, 9-fluorenone, and 9-hydroxyfluorene which were found to ionize via APCI (+), but not APPI (-) used in the targeted analysis of oxyPAHs in water.

RESULTS AND DISCUSSION

Photoproduction of HOPs.

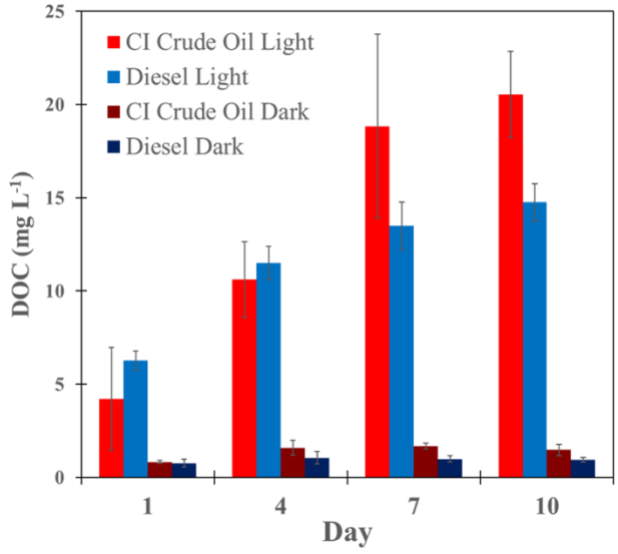

Figure 2. Temporal shifts in DOC for HOPs in all samples. (N = 3, ± SD)

The concentration of DOC is positively correlated with light exposure time (Pearson Correlation Coefficient, $r_{crude} = 0.90$, $r_{diesel} = 0.92$) (**Figure 2**). CI crude oil and diesel samples exposed to light resulted in higher DOC than dark samples ($p < 0.05$ (One-way ANOVA)) (Table A1). Only minor changes in DOC concentrations of dark samples are attributed to readily available water-soluble compounds in petroleum.[70] As time increases, the water-soluble compounds in petroleum can partition into the aqueous phase, resulting in a small increase in DOC.

Light-exposed diesel initially produced higher DOC on days 1 and 4 compared to CI crude oil, where CI crude oil produced more DOC on days 7 and 10. Diesel is a refined fuel that consists of C8-C21 compounds distilled from crude oil. This character can make it more readily photosolubilized compared to whole crude oil. These results match a report by Zito et al. 2019 that showed DOC concentrations produced from a relatively light crude oil increased more rapidly at early irradiation periods. Still, with extended exposure, the DOC from the light crude oil plateaued while that from heavy fuel oil continued to increase.

Optical Characterization of HOPs.

Optical spectroscopy is employed to uncover changes in chromophore composition in HOPs. Table A2 reports spectral indices of the fluorescent dissolved organic matter found in HOPs from each sample. The humification index (HIX) is of particular interest in uncovering compositional trends in HOPs, as it is a general indicator of aromaticity and oxygen content. HIX is derived from the intensity of emission within the ranges 435–480 nm and 300–345 nm with an excitation wavelength of 254 nm.[71] As HIX increases, the ratio of hydrogen to carbon decreases and oxygen content increases.[71] Increasing HIX values represent the relative increase in long-

wavelength, “humified”, water-soluble, oxidized compounds and decrease in short-wavelength compounds. HOPs formed from CI crude oil range in HIX values from 0.58 ± 0.03 at day 1 to 0.66 ± 0.01 at day 10, and HOPs created from diesel range from 0.36 ± 0.02 at day 1 to 0.20 ± 0.01 at day 10. The inverse relationship between the two fuel types suggests that HOPs formed from CI crude oil are more aromatic and oxygenated as time increases. In contrast, HOPs formed from diesel become less aromatic and oxygenated as time increases. Aromaticity and oxygenation trends in diesel and CI crude oil are further explored through non-target molecular characterization techniques discussed later in this report. This relationship can be attributed to compositional differences in the parent petroleum. Crude oil consists of relatively higher molecular weight and aromatic compounds relative to diesel.[72]

Specific UV absorbance at 254 nm ($SUVA_{254}$) is another optical parameter of interest for tracking compositional changes in HOPs as it measures the amount of light-absorbing dissolved organic matter. $SUVA_{254}$ is calculated by dividing absorbance at 254 nm (a_{254}) by the DOC concentration (a_{254} m^{-1}/DOC mg L^{-1}). $SUVA_{254}$ values track compositional changes in HOPs through aromaticity. Increasing $SUVA_{254}$ after light exposure for both fuel types suggest aromatic HOPs are produced.[73] CI crude oil and diesel exposed to light varied in maximum $SUVA_{254}$ (Table A1). CI crude oil $SUVA_{254}$ ranged between 0.0100 ± 0.005 (day 1) and 0.0169 ± 0.001 L mg^{-1} cm^{-1} (day 10). Diesel $SUVA_{254}$ ranged between 0.0108 ± 0.001 (day 1) and 0.0139 ± 0.001 L mg^{-1} cm^{-1} (day 4). The temporal difference of $SUVA_{254}$ maxima for CI crude oil and diesel suggests compositional differences in the photoproduction of HOPs from different fuel sources and time points, which is explored further in detail in this experiment. CI crude oil maximum $SUVA_{254}$ at day 10 suggests aromatic HOPs are produced throughout the total irradiation time, supported by increasing HIX values. Diesel maximum $SUVA_{254}$ on day 4 indicates a decrease in aromatic HOPs production after day 4, which, combined with increasing DOC after day 4, suggests that relatively aliphatic HOPs are produced from days 4-10. These results are consistent with reduced HIX values as both indicate relative loss in aromaticity and could allude to photodegradation of small aromatic molecules to aliphatic-like features. The Whisenhant et al. 2022 study, utilizing high-latitude irradiation conditions, follows similar values for both crude oil (0.009 (day 1) – 0.015 L mg^{-1} cm^{-1} (day 10)) and diesel (0.011 (day 1) – 0.012 L mg^{-1} cm^{-1} (day 10)). These combined results illustrate the photoproduction of diverse compositional HOPs occurs when CI crude oil and diesel are exposed to light.

Parallel factor (PARAFAC) analysis was used to uncover underlying fluorescence components present in the EEMs dataset, allowing for an optical index for tracking compositional changes through the production of HOPs over time. A validated six-component PARAFAC model was derived from the EEMs (**Figure 3a** and A1**).** Component 1 (C1) had excitation and emission (Ex/Em) maxima of 240/374 nm and did not match any other components in the OpenFluor database (>95% similarity score), suggesting a unique HOPs signature is present. Although there were no matches in the OpenFluor database for C1, Ex/Em spectra with similar wavelengths are reported for petroleum degradation products and naphthenic acids (NAs).[74,75] Component 2 (C2

Ex/Em 260/376 nm) (matched 97% similarity score) is consistent with a previous report by Zito et al. (2020)[29], indicating a petroleum-derived DOM signal produced from irradiating heavy and light oils from a surrogate Macondo oil (light) produced after 24 hours. These results show that C2 from this study is indicative of HOPs fluorescent signatures. Component 3 (C3 Ex/Em 270/294 nm), Component 4 (C4 Ex/Em 280/340 nm), and Component 6 (C6 Ex/Em 240/320 nm) matched three, five, and seven entries in the OpenFluor database, respectively. These components are called "tyrosine-like" and "tryptophan-like" ("protein-like) fluorescent signatures in the organic biogeochemistry community.[76-82] However, there are no proteins or amino acids in petroleum. Rather, these fluorescence signatures correspond with relatively reduced (aliphatic, low heteroatom) HOPs.[83,84] Moreover, there are reports of similar fluorescence signatures from water-soluble aliphatic acids photo-oxidation products produced from irradiated oil films and NA standard mixtures.[85,86] Component 5 (C5 Ex/Em 250/460 nm) matched with seven components representing "terrestrial humic-like" fluorescence at a range from 95-96% OpenFluor similarity score.[87-93]

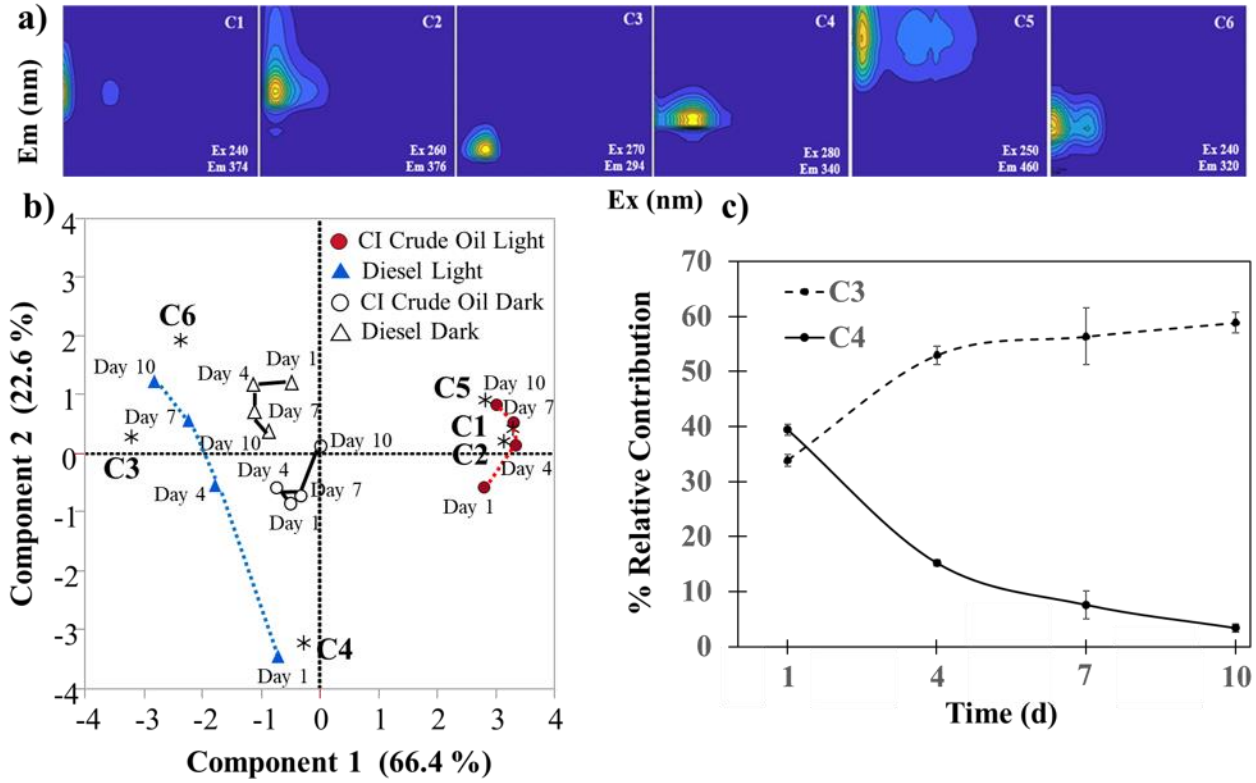

Figure 3. (a) PARAFAC components (b) PCA biplot, loadings represent PARAFAC components. (c) Temporal relationship between C3 and C4 in HOPs formed from light irradiated diesel. (N = 3, ± SD)

Contributions of each component in all samples are reported in Table A3. Principal component analysis shows the relationship between each component and the samples (**Figure 3a**). CI crude oil light samples positively correlate with C1, C2, and C5. Days 4 and 7 are closely related to C2

and C1, respectively, the two petroleum unique components, with C1 being unique to this study (no matches in OpenFluor above). For the CI crude, day 10 is closely related to C5 or the "humic-like" fluorescence that suggests more aromaticity and oxygenation, which aligns with the photodissolution of petroleum. Another interesting relationship is between C4 and C3 and the amount of time diesel is irradiated with light (**Figure 3b)**. C3 represents the production of HOPs, and C4 represents the degradation of parent petroleum compounds. These results show fluorescent signatures can accurately monitor temporal and compositional changes in HOPs.

The HIX values, $SUVA_{254}$ values, and PARAFAC model show a cohesive description of the chemical composition of HOPs formed from CI crude oil and diesel. HOPs produced from CI crude oil are more oxygenated and aromatic in nature, correlating with increasing HIX, increasing $SUVA_{254}$, and long-wavelength "humic-like" fluorescence (C1, C2, C5). HOPs produced from diesel are more reduced and aliphatic, correlating with decreasing HIX, decreasing $SUVA_{254}$, and short-wavelength "protein-like" fluorescence (C3, C4, C6). Optical characterization emphasizes the compositional changes and temporal trends in the formation of HOPs from different petroleum sources.

Molecular Characterization of HOPs.

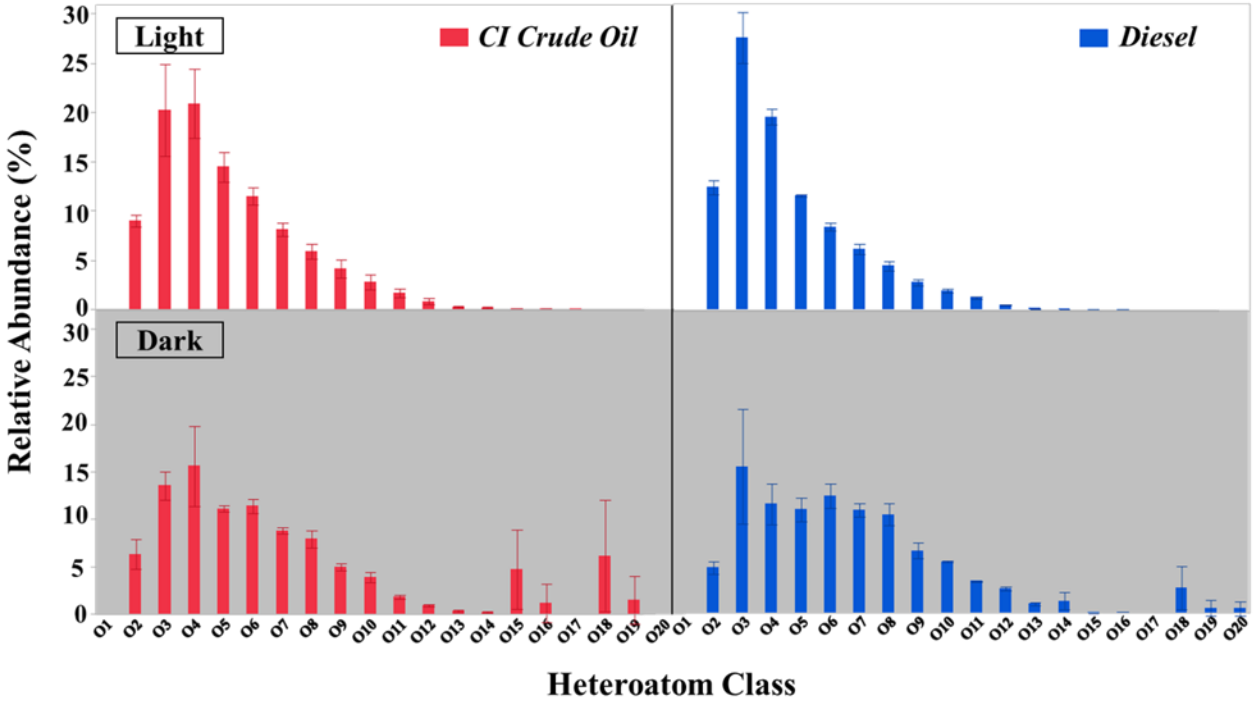

Figure 4. Heteroatom oxygen class graphs from day 10 samples, CI crude oil (red), diesel (blue), irradiated (top), dark (bottom). (N=3, ± SD)

Molecular-level characterization is utilized to further understand the composition of HOPs and complement optical characterization results. Liquid chromatography (LC)-Orbitrap mass

spectrometry was used to characterize the molecular composition of day 4, 7, and 10 sunlight-irradiated CI crude oil and diesel. Heteroatom oxygen class composition uncovers trends in oxygenation (**Figure 4**). CI crude oil and diesel-derived HOPs are composed of compounds that have 2–17 and 2–16 oxygens per molecule, respectively. The most abundant species in CI crude oil derived HOPs and CI crude oil dark control are in the O_4 class. Diesel-derived HOPs and diesel dark controls have the most abundant species in the O_3 class. Dark control samples express the composition of the water-soluble fraction of parent petroleum. The water-soluble compounds from parent petroleum (dark control samples) are composed of compounds that have 2–20 oxygens per molecule. Low concentrations of these compounds can be attributed to the low abundance of polar, water-soluble compounds found in parent petroleum.[94]

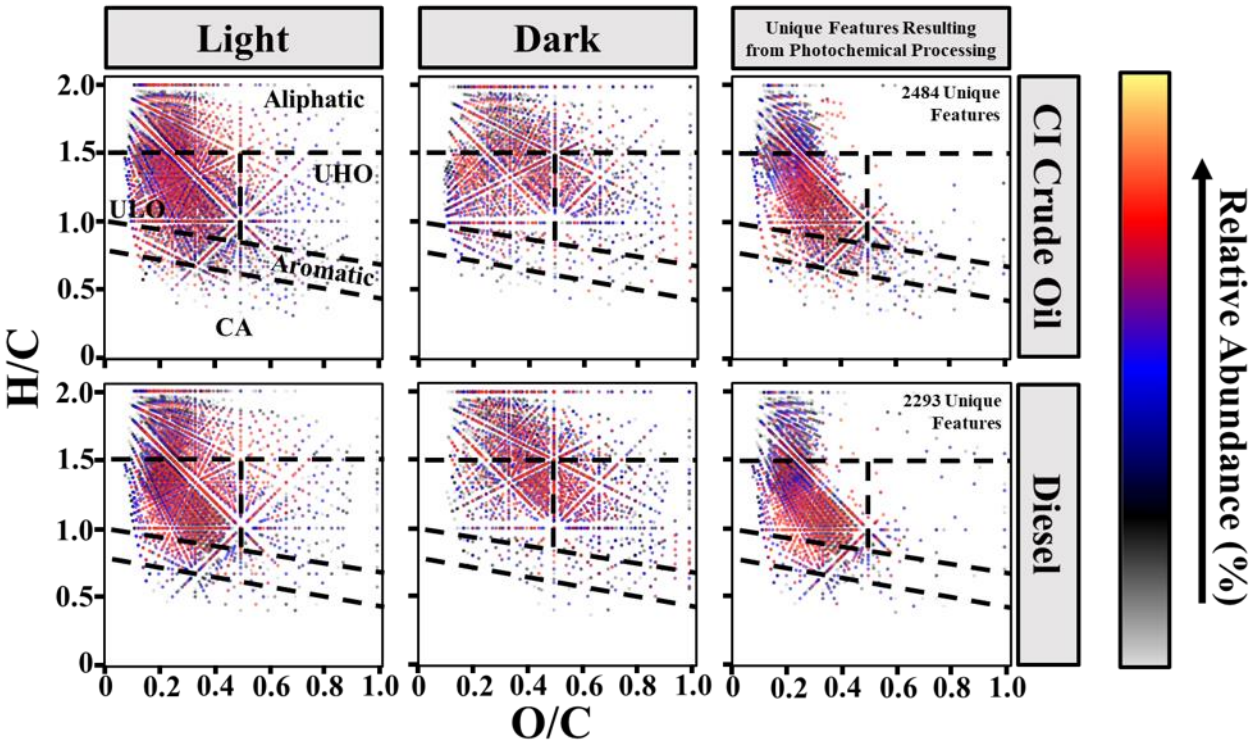

Figure 5. van Krevelen subtraction plots of day 10 dark and light treatments for CI crude oil and diesel where each data point represents a unique molecular feature. Photochemical processing of CI crude oil has 2484 unique features and diesel has 2293 unique features.

A van Krevelen diagram can be used to better characterize HOPs in terms of their molecular composition (**Figure 5**).[95] The dots on the plot represent unique molecular features assigned from mass spectral data with the same O/C and H/C ratios.[96] The diagram can be further decomposed into discrete molecular classification regions (condensed aromatic (CA), aromatic, unsaturated low oxygenation (ULO), unsaturated high oxygenation (UHO), and aliphatic). van Krevelen diagrams can also highlight molecular compositional differences between petroleum source and illumination through a subtraction plot (Figure 5). There are 2,483–2,492 and 1,986–2,293 unique features resulting from photochemical processing in CI crude oil and diesel-derived

HOPs, respectively (Table A4). The unique photochemical features mainly consist of aliphatic (19.21 ± 6.24 – 35.26 ± 20.38 % relative abundance), ULO (48.01 ± 15.10 – 65.14 ± 4.95 % relative abundance), and aromatic (9.93 ± 0.49 – 15.94 ± 2.17 % relative abundance) molecular classifications (Table A5). The molecular composition classifications of HOPs reveal that relatively reduced, saturated, and aromatic compounds are produced by sunlight in high-latitude environments from both CI crude and diesel during summer. The production of CI crude oil and diesel-derived HOPs featuring relatively low oxygenated maximum abundance species (O_4 and O_3, respectively) indicates that relatively reduced compounds are produced.

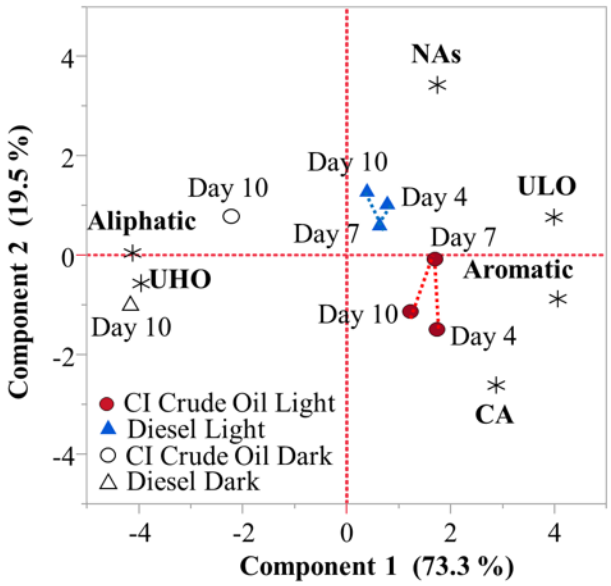

Figure 6. PCA biplot, loadings represent molecular classifications.

Principal component analysis between composition class contributions (Table A5), fuel types, and illumination period was conducted to gain a better understanding of the composition and temporal changes in HOPs (Figure 6). Day 4 light irradiated CI crude oil and diesel produced the highest relative abundance of CA compounds, 4.89 ± 0.17 and 3.07 ± 0.30 %, and aromatic compounds, 11.32 ± 0.37 and 9.46 ± 0.96 %, respectively (Table A4). Day 7 light irradiated CI crude oil and day 10 diesel produced the highest relative abundance of ULO compounds, 47.23 ± 2.05 and 48.61 ± 2.05 %, respectively. Irradiated CI crude oil HOPs consist of slightly more condensed aromatic and aromatic compounds, whereas light irradiated diesel HOPs consist of marginally more ULO compounds. Dark controls for CI crude oil and diesel produced the highest abundance of UHO compounds, 19.18 ± 1.48 and 21.21 ± 2.03 %, respectively, and aliphatic compounds, 39.80 ± 0.75 and 46.11 ± 1.81 %, respectively.

Aliphatic and UHO groups are closely related to the dark samples, while CA, aromatic, NAs, and ULO groups are closely related to the light samples. These trends are consistent with the compositional changes induced by illumination of crude and diesel fuels recently observed with

UHR-MS by Whisenhant et al. (2022). The dark samples consisted of aliphatic and UHO groups due to the readily available water-soluble compounds that the parent petroleum contains.[70] HOPs formed from CI crude oil consisted more of aromatic and CA compounds, whereas HOPs formed from diesel are more aliphatic. Differences between CI crude oil and diesel-produced HOPs come from the compositional differences between the parent petroleum source.[5] The molecular characterization data expresses that dark control samples (representative of the water-soluble compounds in petroleum) are more oxygenated and aliphatic than HOPs. The data also shows HOPs generated from CI crude oil are more aromatic and oxygenated than HOPs generated from diesel, which verifies the results from the optical studies (HIX, $SUVA_{254}$, and PARAFAC).

Although this study focused primarily on photodegradation, it is important to draw comparisons between other major weathering processes, such as biodegradation. Biodegradation of petroleum consists of two major pathways: first, an aerobic process, including enzyme-mediated metabolism and biosynthesis and second, an anoxic process, including anaerobic processes such as fumarate addition, oxygen-independent hydroxylation, and/or carboxylation which forms HOPs.[96-101] The pathways of abiotic vs biotic degradation are both dependent on the specific petroleum composition and the environmental conditions during a spill. Some compound classes such as aromatic hydrocarbons, are known to be more sensitive to photodegradation, whereas saturated hydrocarbons have been shown to be more susceptible to biotic pathways of degradation.[102-108] Podgorski et al. (2021) examined the biodegradation of oil-contaminated groundwater, finding HOPs to exhibit lower relative abundances of condensed aromatics, aliphatics, and unsaturated low oxygen compounds accompanied with an increase of -UHO compounds and no temporal changes in aromatics.[84] Biodegradation products, in general, are less aromatic (2.39–3.57 %)[84] with more UHO (15.5–45.1 %)[84] than the photodegradation products we observed in this study (aromatic: 8.15–11.32 %, UHO: 6.63–8.81 %). Aliphatic hydrocarbons are the most bio-labile class of petroleum.[102, 108, 109] However, both biotic and abiotic pathways are relevant, with the relative pathway contributions being driven by seasonal environmental factors such as temperature, redox potential, water quality, transmittance of light into the water column, seasonality of sunlight exposure, and others.

Detection of OxyPAHs and PAHs in HOPs.

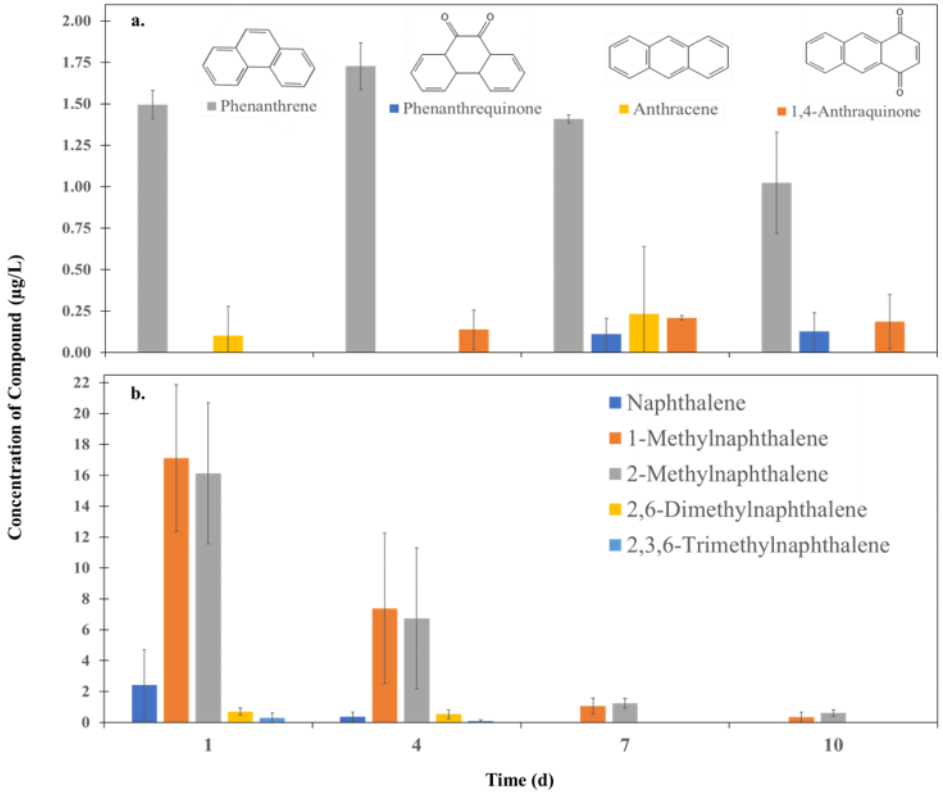

Figure 7. (a) OxyPAHs and their respective PAH derivatives and (b) methylated naphthalene concentrations in HOPs formed from irradiated CI Crude oil. (N=3, ± SD)

A targeted analysis was employed to further understand the composition of HOPs formed through CI crude oil and diesel. LC-QQQ provided quantitation of 8 oxyPAHs, which were correlated to the analysis of 24 PAHs in light-treated samples on days 1, 4, 7, and 10. The oxyPAHs targeted in this analysis consisted of heteroatom oxygen classes between O1-O3. Characterization and quantification of lower oxygenated compounds are of great interest due to their toxicity and abundance in HOPs. Two oxyPAH compounds and 11 PAH compounds were detected (Table A6). The oxyPAHs phenanthrenequinone and 1,4-anthraquinone were present in light-treated CI crude oil HOPs at concentrations of 0.11 ± 0.10 (day 7) - 0.13 ± 0.11 (day 10) and 0.14 ± 0.12 (day 4) - 0.21 ± 0.01 (day 7) µg/L, respectively. OxyPAHs were not detected in the irradiated diesel samples. Acenaphthene is a diesel-unique PAH with no detection in irradiated CI crude oil samples. Anthracene is a CI crude oil unique PAH, with no detection in irradiated diesel samples. The other nine PAH compounds were detected in light-treated CI crude oil and diesel HOPs.

There is an inverse relationship between the oxyPAH, phenanthrenequinone, and its associated PAH, phenanthrene, in irradiated CI crude oil ($p < 0.05$ (One-way ANOVA)) (Figure 7a). Phenanthrene degrades over time, while phenanthrenequinone is produced. This relationship is

consistent with the photooxidation of a PAH to its respective oxyPAH. 1,4-anthraquinone and anthracene do not have a statistically significant relationship ($p > 0.05$ (One-way ANOVA)). However, 1,4-anthraquinone is strongly positively correlated with the amount of time irradiated ($r = 0.87$), suggesting that 1,4-anthraquinone is produced over time. This relationship aligns with more oxidized species being produced with longer irradiation times. Transformations of PAHs to oxyPAHs have been previously reported through photochemical processes.[110,111] Phenanthrenequinone/phenanthrene and 1,4-anthraquinone have potential use for tracking overall degradation and compositional changes in an oil spill event.

Another interesting class of compounds that could be used for monitoring in a spill event is methylated naphthalenes. The concentration of naphthalene-type compounds over time in irradiated CI crude oil can be seen in Figure 7b. The concentration of 1- and 2-methylnaphthalene was greater than the concentration of naphthalene following irradiation of CI crude oil, suggesting that single substituted methylated naphthalenes may be more useful for monitoring CI crude oil dissipation. Future work should include methylated oxyPAHs due to the potential prevalence of other methylated PAHs. Furthermore, methylated PAHs produce transient radical reactive species with relatively greater stability than non-substituted congeners, which may increase the formation of oxidized products. Current efforts include development of a data-dependent tandem mass spectrometry method utilizing MS2 fragmentation to detect additional oxyPAH congeners.

OxyPAHs are a class of compounds that are commonly missed in traditional TPH analysis.[112] The reported results expand on traditional TPH methods by identifying two specific oxyPAHs in crude oil and emphasizing the mixture's complexity due to methylated homologues in both fuel types. Although the list of oxyPAHs and PAHs used in this study is not comprehensive of all the compounds in HOPs formed from CI crude oil and diesel, some promising compounds and relationships can be used to track compositional changes of HOPs for a cheaper and more routine analysis.

Bioaccumulation of oxyPAHs in Mussels.

Measurement of the bioaccumulation of oxyPAHs in mussels was confounded by a high degree of mortality in mussels exposed to diesel HOPs which resulted in fewer mussels available for the assessment of bioaccumulation over the entire exposure period. As diesel is a distillate comprised of lower molecular weight species, the concentration of HOPs that photosolubilized was much higher than that in the crude oil experiments which resulted in a larger HOP dose (60 vs 2 ppm DOC in diesel vs crude oil exposures, respectively) and increased mortality. While the increased bioavailability of diesel relative to crude oil HOPs was apparent, oxyPAHs on our target list were not detected in mussel tissues. While 9-fluorenone may have been present, measured signals in mussels exposed to diesel or crude oil HOPs could not be statistically differentiated from those in mussels exposed to seawater only (Figure 8). These findings corroborate the results of our targeted analysis of oxyPAHs in water which suggest that

methylated congeners may contribute more to the overall mixture of HOPs than the non-substituted congeners that were available as analytical standards for this work.

We believe that the reason we did not detect any oxyPAHs in mussel tissues is because the compounds which bioaccumulated are 1) not available as reference standards and 2) were not the degradation products of the specific PAHs we have on our target list. Therefore, we conclude that the bioaccumulation potential of photo-solubilized oil cannot be easily accomplished by traditional targeted methods. On the other hand, our non-targeted approach provides insight into which 'chemical features' (e.g., aliphatic, aromatic, etc.) are present and how these chemical features change over time. However, it does not provide compound-specific information, which is what traditional water quality criteria are based on. Therefore, traditional compliance-based monitoring programs that utilize targeted approaches (analysis of a pre-set list of compounds) are not adequate for HOP bioaccumulation. We suggest that non-target analyses using emerging tools such as fragmentation spectra from high-resolution mass spectrometry be further investigated to assess this knowledge gap.

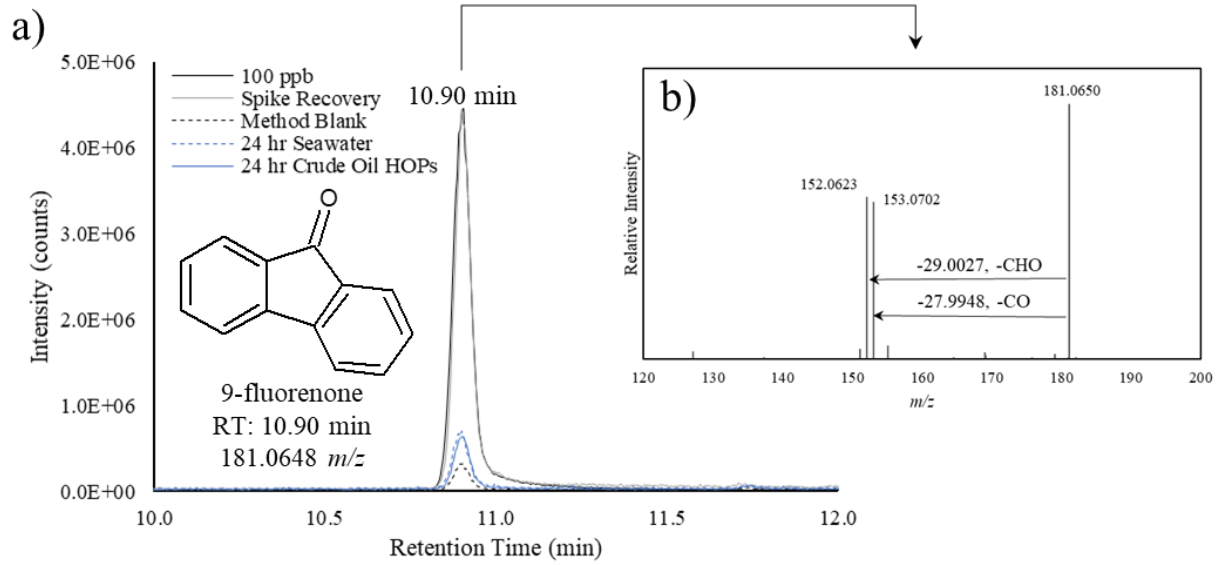

Figure 8. Mussel tissue analyses of oxyPAHs. (a) Detection of 9-fluorenone by LC-Orbitrap confirms good spike recovery of 9-fluorenone with trace detection in samples and method blank. Unfortunately, detections in mussels exposed to HOPs could not be distinguished from background seawater controls. (b) Product ion spectrum for 9-fluorenone positively confirms compound identity based on the characteristic fragmentation of the precursor ion (181.0650 *m/z*).

CONCLUSIONS

This study identifies HOP formation resulting from irradiation of both CI crude oil and diesel over simulated seawater using simulated environmental conditions of the sub-Arctic. DOC measurements confirmed that sunlight irradiation mobilizes petrogenic carbon into seawater. Six

unique fluorescence EEM components were identified in irradiated HOPs, ranging across reduced and oxidized compounds. Irradiated seawater produced greater abundances of CA, aromatic, and ULO chemical features and higher oxyPAH loads predominated by phenanthrenequinone and 1,4-anthraquinone. While the toxicological significance of HOPs is still an emerging research area, the production of HOPs, which this study identifies, could have important toxicological implications during an oil spill event. This report details findings corresponding to high-latitude regions during the summer, but has general implications for monitoring HOPs in any region.

ACKNOWLEDGMENTS

Funding from this project was provided by U.S. Department of Interior, Bureau of Ocean Energy Management Environmental Studies Program (BOEM Cooperative Agreement M20AC10012) to P. Tomco through the University of Alaska Coastal Marine Institute and National Science Foundation Award number 1929173 to P. Tomco. We are grateful for matching support from ConocoPhillips Arctic Science and Engineering Endowment. Maxwell Harsha was supported by an Oil Spill Recovery Institute Graduate Research Fellowship (22-10-09).

STUDY PRODUCTS

Publications.

Whisenhant, E. A., Zito, P., Podgorski, D. C., McKenna, A. M., Redman, Z. C., & Tomco, P. L. (2022). Unique Molecular Features of Water-Soluble Photo-Oxidation Products among Refined Fuels, Crude Oil, and Herded Burnt Residue under High Latitude Conditions. *ACS ES&T Water*, *2*(6), 994-1002.

Harsha, M. L., Redman, Z. C., Wesolowski, J., Podgorski, D. C., & Tomco, P. L. (2023). Photochemical formation of water-soluble oxyPAHs, naphthenic acids, and other hydrocarbon oxidation products from Cook Inlet, Alaska crude oil and diesel in simulated seawater spills. *Environmental Science: Advances*, *2*(3), 447-461.

Presentations.

Podgorski, D.C; Harsha, M.L.; Verna, D.; Redman, Z.C.; Fouche, A.; Wesolowski, J.; Tomco, P.L. The Unresolved Complex Mixture: Dissolved Hydrocarbon Oxidation Products are the Final Frontier in Understanding Transport, Fate, and Ecological Impacts of High Latitude Oil Spills. 2023 (*accepted abstract)* AMOP Technical Seminar, Oral Presentation.

Harsha, M.L.; Verna, D.; Redman, Z.C.; Wesolowski, J.; Fouche, A.; Podgorski, D.C.; Tomco, P.L. Uncovering the Fate of High Latitude Oil Spills: Non-target LC-Orbitrap Analysis of Hydrocarbon Oxidation Products. 2023 (*accepted abstract*) ASMS Meeting, Oral Presentation.

Redman, Z., Podgorski, D., Fouche, A., Harsha, M., and Tomco, P. Liquid chromatography tandem mass spectrometry with photo ionization for the determination of parent and oxyPAHs in seawater and mussels following the photooxidation of simulated oil spills. ACS San Diego National Meeting, Spring 2022. Oral Presentation

Harsha, M., Redman, Z., Fouche, A., Wesolowski, J., Podgorski, D., and Tomco, P., Photochemical formation and subsequent bioaccumulation of hydrocarbon oxidation products from high latitude oil spills ACS Chicago National Meeting, Fall 2022. Oral Presentation

Fouche, A., Harsha, M., and Tomco, P., Hydrocarbon Oxidation Products in Cook Inlet: Formation and Bioaccumulation., Invited presentation to Cook Inlet Regional Citizens Advisory Council, November 2022.

REFERENCES

1. Bureau of Ocean Energy Management (2016). Cook Inlet Planning Area Oil and Gas Lease Sale 244, Final Environmental Impact Statement. 2 Volumes. OCS EIS/EA BOEM 2016-069. Anchorage, AK: USDOI, BOEM, Alaska OCS Region.

2. Aeppli, C., Carmichael, C.A., Nelson, R.K., Lemkau, K.L., Graham, W.M., Redmond, M.C., Valentine, D.L., Reddy, C.M., (2012). Oil Weathering after the Deepwater Horizon Disaster Led to the Formation of Oxygenated Residues. *Environmental Science & Technology,* 46, 8799-8807.

3. Amos, R. T., Bekins, B. A., Cozzarelli, I. M., Voytek, M. A., Kirshtein, J. D., Jones, E. J. P., Blowes, D. W., (2012). Evidence for iron-mediated anaerobic methane oxidation in a crude oil-contaminated aquifer. *Geobiology,* 10, 506-517.

4. Hazen, T. C., Prince, R. C., Mahmoudi, N., (2016). Marine Oil Biodegradation. *Environmental Science & Technology,* 50, 2121-2129.

5. McFarlin, K. M., Prince, R. C., Perkins, R., & Leigh, M. B. (2014). Biodegradation of dispersed oil in Arctic seawater at -1 C. PloS one, 9(1), e84297

6. Townsend, G. T., Prince, R. C., Suflita, J. M., (2003). Anaerobic oxidation of crude oil hydrocarbons by the resident microorganisms of a contaminated anoxic aquifer. *Environmental Science & Technology,* 37, 5213-5218.

7. Bekins, B. A., Cozzarelli, I. M., Erickson, M. L., Steenson, R. A., Thorn, K. A., (2016). Crude Oil Metabolites in Groundwater at Two Spill Sites. *Groundwater,* 54, 681-691.

8. Essaid, H. I., Bekins, B. A., Herkelrath, W. N., Delin, G. N., (2011). Crude Oil at the Bemidji Site: 25 Years of Monitoring, Modeling, and Understanding. *Groundwater*, 49, 706-726.

9. Zito, P., Ghannam, R., Bekins, B. A., & Podgorski, D. C. (2019a). Examining the Extraction Efficiency of Petroleum-Derived Dissolved Organic Matter in Contaminated Groundwater Plumes. *Groundwater Monitoring & Remediation*, *39*(4), 25-31.

10. Carney, M. W., Erwin, K., Hardman, R., Yuen, B., Volz, D. C., Hinton, D. E., Kullman, S. W., (2008). Differential developmental toxicity of naphthoic acid isomers in medaka (Oryzias latipes) embryos. *Marine Pollution Bulletin*, 57, 255-266.

11. Lundstedt, S., White, P .A., Lemieux, C. L., Lynes, K. D., Lambert, L. B., Oberg, L., Haglund, P., Tysklind, M., (2007). Sources, fate, and toxic hazards of oxygenated polycyclic aromatic hydrocarbons (PAHs) at PAH-contaminated sites. *Ambio,* 36, 475-485.

12. Wincent, E., Jonsson, M. E., Bottai, M., Lundstedt, S., Dreij, K., (2015). Aryl Hydrocarbon Receptor Activation and Developmental Toxicity in Zebrafish in Response to Soil Extracts Containing Unsubstituted and Oxygenated PAHs. *Environmental Science & Technology,* 49, 3869-3877.

13. National Research Council, (2003). Oil in the Sea III: Inputs, Fates, and Effects, Committee on Oil in the Sea: Inputs, Fates, and Effects, Ocean Studies Board and Marine Board,

Divisions of Earth and Life Studies and Transportation Research Board, National Research Council, National Academies Press, Washington, D.C. 277 pp.

14. Podgorski, D. C., Zito, P., McGuire, J. T., Martinovic-Weigelt, D., Cozzarelli, I. M., Bekins, B. A., & Spencer, R. G. (2018). Examining Natural Attenuation and Acute Toxicity of Petroleum-Derived Dissolved Organic Matter with Optical Spectroscopy. *Environmental science & technology*, *52*(11), 6157-6166.

15. Brack, W., Altenburger, R., Küster, E., Meissner, B., Wenzel, K. D., & Schüürmann, G. (2003). Identification of toxic products of anthracene photomodification in simulated sunlight. *Environmental Toxicology and Chemistry: An International Journal*, *22*(10), 2228-2237.

16. Idowu, O., Semple, K. T., Ramadass, K., O'Connor, W., Hansbro, P., & Thavamani, P. (2019). Beyond the obvious: Environmental health implications of polar polycyclic aromatic hydrocarbons. *Environment international*, *123*, 543-557.

17. Layshock, J. A., Wilson, G., & Anderson, K. A. (2010). Ketone and quinone-substituted polycyclic aromatic hydrocarbons in mussel tissue, sediment, urban dust, and diesel particulate matrices. *Environmental toxicology and chemistry*, *29*(11), 2450-2460.

18. Lundstedt, S., White, P .A., Lemieux, C. L., Lynes, K. D., Lambert, L. B., Oberg, L., Haglund, P., Tysklind, M., (2007). Sources, fate, and toxic hazards of oxygenated polycyclic aromatic hydrocarbons (PAHs) at PAH-contaminated sites. *Ambio*, 36, 475-485.

19. Tidwell, L. G., Allan, S. E., O'Connell, S. G., Hobbie, K. A., Smith, B. W., & Anderson, K. A. (2016). PAH and OPAH flux during the deepwater horizon incident. *Environmental science & technology*, *50*(14), 7489-7497.

20. G. S. Frysinger, R. B. Gaines, L. Xu and C. M. Reddy, (2003). Resolving the Unresolved Complex Mixture in Petroleum-Contaminated Sediments, *Environmental Science & Technology*, **37**, 1653-1662.

21. L. C. Krajewski, R. P. Rodgers and A. G. Marshall, 126 264 Assigned Chemical Formulas from an Atmospheric Pressure Photoionization 9.4 T Fourier Transform Positive Ion Cyclotron Resonance Mass Spectrum, *Analytical Chemistry*, 2017, **89**, 11318-11324.

22. D. C. Palacio Lozano, R. Gavard, J. P. Arenas-Diaz, M. J. Thomas, D. D. Stranz, E. Mejía-Ospino, A. Guzman, S. E. F. Spencer, D. Rossell and M. P. Barrow, Pushing the analytical limits: new insights into complex mixtures using mass spectra segments of constant ultrahigh resolving power, *Chemical Science*, 2019, **10**, 6966-6978.

23. G. Isaacman, K. R. Wilson, A. W. H. Chan, D. R. Worton, J. R. Kimmel, T. Nah, T. Hohaus, M. Gonin, J. H. Kroll, D. R. Worsnop and A. H. Goldstein, Improved Resolution of Hydrocarbon Structures and Constitutional Isomers in Complex Mixtures Using Gas Chromatography-Vacuum Ultraviolet-Mass Spectrometry, *Analytical Chemistry*, 2012, **84**, 2335-2342.

24. A. M. McKenna, R. K. Nelson, C. M. Reddy, J. J. Savory, N. K. Kaiser, J. E. Fitzsimmons, A. G. Marshall and R. P. Rodgers, Expansion of the Analytical Window for Oil Spill Characterization by Ultrahigh Resolution Mass Spectrometry: Beyond Gas Chromatography, *Environmental Science & Technology*, 2013, **47**, 7530-7539.

25. S. F. Niles, M. L. Chacón-Patiño, H. Chen, A. M. McKenna, G. T. Blakney, R. P. Rodgers and A. G. Marshall, Molecular-Level Characterization of Oil-Soluble Ketone/Aldehyde Photo-Oxidation Products by Fourier Transform Ion Cyclotron Resonance Mass Spectrometry Reveals Similarity Between Microcosm and Field Samples, *Environmental Science & Technology*, 2019, **53**, 6887-6894.

26. B. M. Ruddy, C. L. Hendrickson, R. P. Rodgers and A. G. Marshall, Positive Ion Electrospray Ionization Suppression in Petroleum and Complex Mixtures, *Energy & Fuels*, 2018, **32**, 2901-2907.

27. B. M. Ruddy, M. Huettel, J. E. Kostka, V. V. Lobodin, B. J. Bythell, A. M. McKenna, C. Aeppli, C. M. Reddy, R. K. Nelson, A. G. Marshall and R. P. Rodgers, Targeted Petroleomics: Analytical Investigation of Macondo Well Oil Oxidation Products from Pensacola Beach, *Energy & Fuels*, 2014, **28**, 4043-4050.

28. S. A. Wise, R. P. Rodgers, C. M. Reddy, R. K. Nelson, E. B. Kujawinski, T. L. Wade, A. D. Campiglia and Z. Liu, Advances in Chemical Analysis of Oil Spills Since the Deepwater Horizon Disaster, *Critical Reviews in Analytical Chemistry*, 2022, DOI: 10.1080/10408347.2022.2039093, 1-60.

29. P. Zito, D. C. Podgorski, T. Bartges, F. Guillemette, J. A. Roebuck, R. G. M. Spencer, R. P. Rodgers and M. A. Tarr, Sunlight-Induced Molecular Progression of Oil into Oxidized Oil Soluble Species, Interfacial Material, and Dissolved Organic Matter, *Energy & Fuels*, 2020, **34**, 4721-4726.

30. B. De Witte, C. Walgraeve, K. Demeestere and H. Van Langenhove, Oxygenated polycyclic aromatic hydrocarbons in mussels: analytical method development and occurrence in the Belgian coastal zone, *Environmental Science and Pollution Research*, 2019, **26**, 9065-9078.

31. H. P. H. Arp, S. Lundstedt, S. Josefsson, G. Cornelissen, A. Enell, A.-S. Allard and D. B. Kleja, Native OxyPAHs, N-PACs, and PAHs in Historically Contaminated Soils from Sweden, Belgium, and France: Their Soil-Porewater Partitioning Behavior, Bioaccumulation in Enchytraeus crypticus, and Bioavailability, *Environmental Science & Technology*, 2014, **48**, 11187-11195.

32. S. Josefsson, H. P. H. Arp, D. B. Kleja, A. Enell and S. Lundstedt, Determination of polyoxymethylene (POM) – water partition coefficients for oxyPAHs and PAHs, *Chemosphere*, 2015, **119**, 1268-1274.

33. C. L. Lemieux, I. B. Lambert, S. Lundstedt, M. Tysklind and P. A. White, Mutagenic hazards of complex polycyclic aromatic hydrocarbon mixtures in contaminated soil, *Environmental Toxicology and Chemistry*, 2008, **27**, 978-990.

34. S. Lundstedt, P. A. White, C. L. Lemieux, K. D. Lynes, I. B. Lambert, L. Öberg, P. Haglund and M. Tysklind, Sources, Fate, and Toxic Hazards of Oxygenated Polycyclic Aromatic Hydrocarbons (PAHs) at PAH- contaminated Sites, *AMBIO: A Journal of the Human Environment*, 2007, **36**, 475-485, 411.

35. E. Wincent, M. E. Jönsson, M. Bottai, S. Lundstedt and K. Dreij, Aryl Hydrocarbon Receptor Activation and Developmental Toxicity in Zebrafish in Response to Soil Extracts Containing Unsubstituted and Oxygenated PAHs, *Environmental Science & Technology*, 2015, **49**, 3869-3877.

36. Blackburn, M., Mazzacano, C., Fallon, C., and Black, S. (2014) Oil in our oceans: A review of the impacts of oil spills on marine invertebrates. 152 pp. 1st ed. Portland, OR: The Xerces Society for Invertebrate Conservation.

37. Mundy, P. R., & Cooney, R. T. (2005). Physical and biological background. P. R. Mundy, ed. *The Gulf of Alaska: Biology and oceanography. Alaska Sea Grant College Program, University of Alaska, Fairbanks, Alaska*, 15-23.

38. Kautsky, N. (1982). Quantitative studies on gonad cycle, fecundity, reproductive output and recruitment in a Baltic Mytilus edulis population. *Marine Biology*, *68*(2), 143-160.

39. Barron, M. G., & Ka'aihue, L. (2001). Potential for photoenhanced toxicity of spilled oil in Prince William Sound and Gulf of Alaska waters. *Marine pollution bulletin*, *43*(1-6), 86-92.

40. Almeda, R., Harvey, T. E., Connelly, T. L., Baca, S., & Buskey, E. J. (2016). Influence of UVB radiation on the lethal and sublethal toxicity of dispersed crude oil to planktonic copepod nauplii. *Chemosphere*, *152*, 446-458.

41. Finch, B. E., Stefansson, E. S., Langdon, C. J., Pargee, S. M., Blunt, S. M., Gage, S. J., & Stubblefield, W. A. (2016a). Photo-enhanced toxicity of two weathered Macondo crude oils to early life stages of the eastern oyster (Crassostrea virginica). *Marine pollution bulletin*, *113*(1-2), 316-323.

42. Damare, L. M., Bridges, K. N., Alloy, M. M., Curran, T. E., Soulen, B. K., Forth, H. P., ... & Roberts, A. P. (2018). Photo-induced toxicity in early life stage fiddler crab (Uca longisignalis) following exposure to Deepwater Horizon oil. *Ecotoxicology*, *27*(4), 440-447.

43. Alloy, M., Baxter, D., Stieglitz, J., Mager, E., Hoenig, R., Benetti, D., ... & Roberts, A. (2016). Ultraviolet radiation enhances the toxicity of Deepwater Horizon oil to mahi-mahi (Coryphaena hippurus) embryos. *Environmental science & technology*, *50*(4), 2011-2017.

44. Finch, B. E., & Stubblefield, W. A. (2016b). Photo-enhanced toxicity of fluoranthene to Gulf of Mexico marine organisms at different larval ages and ultraviolet light intensities. *Environmental toxicology and chemistry*, *35*(5), 1113-1122.

45. Pelletier, M., Burgess, R., Ho, K., Kuhn, A., McKinney, R., & Ryba, S., (2009). Phototoxicity of individual polycyclic aromatic hydrocarbons and petroleum to marine invertebrate larvae and juveniles. *Environmental Toxicology and Chemistry*, 16(10), 2190-2199.

46. Barron, M., (2017). Photoenhanced toxicity of petroleum to aquatic invertebrates and fish. A*rchives of Environmental Contamination and Toxicology*, 73, 40-46.

47. Pelletier, M., Burgess, R., Ho, K., Kuhn, A., McKinney, R., & Ryba, S., (2009). Phototoxicity of individual polycyclic aromatic hydrocarbons and petroleum to marine invertebrate larvae and juveniles. *Environmental Toxicology and Chemistry*, 16(10), 2190-2199.

48. Berenshtein, I., Paris, C. B., Perlin, N., Alloy, M. M., Joye, S. B., & Murawski, S. (2020). Invisible oil beyond the Deepwater Horizon satellite footprint. *Science advances*, *6*(7), eaaw8863.

49. D. Dissing and G. Wendler, Solar Radiation Climatology of Alaska, *Theoretical and Applied Climatology*, 1998, **61**, 161-175.

50. M. Atkinson and C. Bingman, Elemental composition of commercial seasalts, *Journal of Aquariculture and Aquatic Sciences*, 1997, **8**, 39-43.

51. A. Stubbins and T. Dittmar, Low volume quantification of dissolved organic carbon and dissolved nitrogen, *Limnology and Oceanography: Methods*, 2012, **10**, 347-352.

52. R. G. M. Spencer, L. Bolton and A. Baker, Freeze/thaw and pH effects on freshwater dissolved organic matter fluorescence and absorbance properties from a number of UK locations, *Water Research*, 2007, **41**, 2941-2950.

53. M. M. Tfaily, D. C. Podgorski, J. E. Corbett, J. P. Chanton and W. T. Cooper, Influence of acidification on the optical properties and molecular composition of dissolved organic matter, *Analytica Chimica Acta*, 2011, **706**, 261-267.

54. M. Yan, Q. Fu, D. Li, G. Gao and D. Wang, Study of the pH influence on the optical properties of dissolved organic matter using fluorescence excitation–emission matrix and parallel factor analysis, *Journal of Luminescence*, 2013, **142**, 103-109.

55. P. Kowalczuk, W. J. Cooper, R. F. Whitehead, M. J. Durako and W. Sheldon, Characterization of CDOM in an organic-rich river and surrounding coastal ocean in the South Atlantic Bight, *Aquatic Sciences*, 2003, **65**, 384-401.

56. T. Ohno, Fluorescence Inner-Filtering Correction for Determining the Humification Index of Dissolved Organic Matter, *Environmental Science & Technology*, 2002, **36**, 742-746.

57. K. R. Murphy, C. A. Stedmon, D. Graeber and R. Bro, Fluorescence spectroscopy and multi-way techniques. PARAFAC, *Analytical Methods*, 2013, **5**, 6557-6566.

58. R. A. Harshman and M. E. Lundy, PARAFAC: Parallel factor analysis, *Computational Statistics & Data Analysis*, 1994, **18**, 39-72.

59. C. A. Stedmon and R. Bro, Characterizing dissolved organic matter fluorescence with parallel factor analysis: a tutorial, *Limnology and Oceanography: Methods*, 2008, **6**, 572-579.

60. K. R. Murphy, C. A. Stedmon, P. Wenig and R. Bro, OpenFluor– an online spectral library of auto-fluorescence by organic compounds in the environment, *Analytical Methods*, 2014, **6**, 658-661.

61. T. Dittmar, B. Koch, N. Hertkorn and G. Kattner, A simple and efficient method for the solid-phase extraction of dissolved organic matter (SPE-DOM) from seawater, *Limnology and Oceanography: Methods*, 2008, **6**, 230-235.

62. P. Zito, R. Ghannam, B. A. Bekins and D. C. Podgorski, Examining the Extraction Efficiency of Petroleum-Derived Dissolved Organic Matter in Contaminated Groundwater Plumes, *Groundwater Monitoring & Remediation*, 2019, **39**, 25-31.

63. J. A. Hawkes, J. D'Andrilli, J. N. Agar, M. P. Barrow, S. M. Berg, N. Catalán, H. Chen, R. K. Chu, R. B. Cole, T. Dittmar, R. Gavard, G. Gleixner, P. G. Hatcher, C. He, N. J. Hess, R. H. S. Hutchins, A. Ijaz, H. E. Jones, W. Kew, M. Khaksari, D. C. Palacio Lozano, J. Lv, L. R. Mazzoleni, B. E. Noriega-Ortega, H. Osterholz, N. Radoman, C. K. Remucal, N. D. Schmitt, S. K. Schum, Q. Shi, C. Simon, G. Singer, R. L. Sleighter, A. Stubbins, M. J. Thomas, N. Tolic, S. Zhang, P. Zito and D. C. Podgorski, An international laboratory comparison of dissolved organic matter composition by high resolution mass spectrometry: Are we getting the same answer?, *Limnology and Oceanography: Methods*, 2020, **18**, 235-258.

64. T. P. Fan, Characterization of naphthenic acids in petroleum by fast atom bombardment mass spectrometry, *Energy & Fuels*, 1991, **5**, 371-375.

65. F. M. Holowenko, M. D. MacKinnon and P. M. Fedorak, Characterization of naphthenic acids in oil sands wastewaters by gas chromatography-mass spectrometry, *Water Research*, 2002, **36**, 2843-2855.

66. B. P. Koch and T. Dittmar, From mass to structure: an aromaticity index for high-resolution mass data of natural organic matter, *Rapid Communications in Mass Spectrometry*, 2006, **20**, 926-932.

67. J. A. O'Donnell, G. R. Aiken, K. D. Butler, F. Guillemette, D. C. Podgorski and R. G. M. Spencer, DOM composition and transformation in boreal forest soils: The effects of temperature and organic-horizon decomposition state, *Journal of Geophysical Research: Biogeosciences*, 2016, **121**, 2727-2744.

68. T. Šantl-Temkiv, K. Finster, T. Dittmar, B. M. Hansen, R. Thyrhaug, N. W. Nielsen and U. G. Karlson, Hailstones: A Window into the Microbial and Chemical Inventory of a Storm Cloud, *PLOS ONE*, 2013, **8**, e53550.

69. M. Guiñez, C. Bazan, L. D. Martinez and S. Cerutti, Determination of nitrated and oxygenated polycyclic aromatic hydrocarbons in water samples by a liquid–liquid phase microextraction procedure based on the solidification of a floating organic drop followed by solvent assisted back-extraction and liquid chromatography–tandem mass spectrometry, *Microchemical Journal*, 2018, **139**, 164-173.

70. M. Eftekhardadkhah and G. Øye, Correlations between Crude Oil Composition and Produced Water Quality: A Multivariate Analysis Approach, *Industrial & Engineering Chemistry Research*, 2013, **52**, 17315-17321.

71. A. Zsolnay, E. Baigar, M. Jimenez, B. Steinweg and F. Saccomandi, Differentiating with fluorescence spectroscopy the sources of dissolved organic matter in soils subjected to drying, *Chemosphere*, 1999, **38**, 45-50.

72. B. P. Hollebone, Oil Physical Properties in Fingas, M. ed. *Handbook of Oil Spill Science and Technology*, 2014, DOI: https://doi.org/10.1002/9781118989982.ch2, pp. 37-50.

73. J. L. Weishaar, G. R. Aiken, B. A. Bergamaschi, M. S. Fram, R. Fujii and K. Mopper, Evaluation of Specific Ultraviolet Absorbance as an Indicator of the Chemical Composition and Reactivity of Dissolved Organic Carbon, *Environmental Science & Technology*, 2003, **37**, 4702-4708.

74. Z. Zhou, L. Guo, A. M. Shiller, S. E. Lohrenz, V. L. Asper and C. L. Osburn, Characterization of oil components from the Deepwater Horizon oil spill in the Gulf of Mexico using fluorescence EEM and PARAFAC techniques, *Marine Chemistry*, 2013, **148**, 10-21.

75. M. H. Mohamed, L. D. Wilson, J. V. Headley and K. M. Peru, Screening of oil sands naphthenic acids by UV-Vis absorption and fluorescence emission spectrophotometry, *Journal of Environmental Science and Health, Part A*, 2008, **43**, 1700-1705.

76. C. A. Stedmon and S. Markager, Tracing the production and degradation of autochthonous fractions of dissolved organic matter by fluorescence analysis, *Limnology and Oceanography*, 2005, **50**, 1415-1426.

77. S. Retelletti Brogi, G. Cossarini, G. Bachi, C. Balestra, E. Camatti, R. Casotti, G. Checcucci, S. Colella, V. Evangelista, F. Falcini, F. Francocci, T. Giorgino, F. Margiotta,

M. Ribera d'Alcalà, M. Sprovieri, S. Vestri and C. Santinelli, Evidence of Covid-19 lockdown effects on riverine dissolved organic matter dynamics provides a proof-of-concept for needed regulations of anthropogenic emissions, *Science of The Total Environment*, 2022, **812**, 152412.

78. K. R. Murphy, G. M. Ruiz, W. T. M. Dunsmuir and T. D. Waite, Optimized Parameters for Fluorescence-Based Verification of Ballast Water Exchange by Ships, *Environmental Science & Technology*, 2006, **40**, 2357-2362.

79. K. R. Murphy, A. Hambly, S. Singh, R. K. Henderson, A. Baker, R. Stuetz and S. J. Khan, Organic Matter Fluorescence in Municipal Water Recycling Schemes: Toward a Unified PARAFAC Model, *Environmental Science & Technology*, 2011, **45**, 2909-2916.

80. K. Lu, H. Gao, H. Yu, D. Liu, N. Zhu and K. Wan, Insight into variations of DOM fractions in different latitudinal rural black-odor waterbodies of eastern China using fluorescence spectroscopy coupled with structure equation model, *Science of The Total Environment*, 2022, **816**, 151531.

81. M. H. Jeon, J. Jung, M. O. Park, S. Aoki, T.-W. Kim and S.-K. Kim, Tracing Circumpolar Deep Water and glacial meltwater using humic-like fluorescent dissolved organic matter in the Amundsen Sea, Antarctica, *Marine Chemistry*, 2021, **235**, 104008.

82. C. DeFrancesco and C. Guéguen, Long-term Trends in Dissolved Organic Matter Composition and Its Relation to Sea Ice in the Canada Basin, Arctic Ocean (2007–2017), *Journal of Geophysical Research: Oceans*, 2021, **126**, e2020JC016578.

83. D. C. Podgorski, P. Zito, J. T. McGuire, D. Martinovic-Weigelt, I. M. Cozzarelli, B. A. Bekins and R. G. M. Spencer, Examining Natural Attenuation and Acute Toxicity of Petroleum-Derived Dissolved Organic Matter with Optical Spectroscopy, *Environmental Science & Technology*, 2018, **52**, 6157-6166.

84. D. C. Podgorski, P. Zito, A. M. Kellerman, B. A. Bekins, I. M. Cozzarelli, D. F. Smith, X. Cao, K. Schmidt-Rohr, S. Wagner, A. Stubbins and R. G. M. Spencer, Hydrocarbons to carboxyl-rich alicyclic molecules: A continuum model to describe biodegradation of petroleum-derived dissolved organic matter in contaminated groundwater plumes, *Journal of Hazardous Materials*, 2021, **402**, 123998.

85. M. C. R. Remolina, Z. Li and N. M. Peleato, Application of machine learning methods for rapid fluorescence-based detection of naphthenic acids and phenol in natural surface waters, *Journal of Hazardous Materials*, 2022, **430**, 128491.

86. F. Berthou, J. Ducreux and G. Bodennec, Analysis of Water-Soluble Acidic Compounds Derived from Spilled Oil in a Controlled Marine Enclosure, *International Journal of Environmental Analytical Chemistry*, 1985, **21**, 267-282.

87. C. A. Stedmon, S. Markager, L. Tranvik, L. Kronberg, T. Slätis and W. Martinsen, Photochemical production of ammonium and transformation of dissolved organic matter in the Baltic Sea, *Marine Chemistry*, 2007, **104**, 227-240.

88. M. Søndergaard, C. A. Stedmon and N. H. Borch, Fate of terrigenous dissolved organic matter (DOM) in estuaries: Aggregation and bioavailability, *Ophelia*, 2003, **57**, 161-176.

89. M. A. Smith, J. S. Kominoski, E. E. Gaiser, R. M. Price and T. G. Troxler, Stormwater Runoff and Tidal Flooding Transform Dissolved Organic Matter Composition and Increase Bioavailability in Urban Coastal Ecosystems, *Journal of Geophysical Research: Biogeosciences*, 2021, **126**, e2020JG006146.

90. A.-R. Schittich, U. J. Wünsch, H. V. Kulkarni, M. Battistel, H. Bregnhøj, C. A. Stedmon and U. S. McKnight, Investigating Fluorescent Organic-Matter Composition as a Key Predictor for Arsenic Mobility in Groundwater Aquifers, *Environmental Science & Technology*, 2018, **52**, 13027-13036.

91. D. Graeber, Y. Tenzin, M. Stutter, G. Weigelhofer, T. Shatwell, W. von Tümpling, J. Tittel, A. Wachholz and D. Borchardt, Bioavailable DOC: reactive nutrient ratios control heterotrophic nutrient assimilation—An experimental proof of the macronutrient-access hypothesis, *Biogeochemistry*, 2021, **155**, 1-20.

92. M. Derrien, M.-S. Kim, G. Ock, S. Hong, J. Cho, K.-H. Shin and J. Hur, Estimation of different source contributions to sediment organic matter in an agricultural-forested watershed using end member mixing analyses based on stable isotope ratios and fluorescence spectroscopy, *Science of The Total Environment*, 2018, **618**, 569-578.

93. T. B. Bittar, S. A. Berger, L. M. Birsa, T. L. Walters, M. E. Thompson, R. G. M. Spencer, E. L. Mann, A. Stubbins, M. E. Frischer and J. A. Brandes, Seasonal dynamics of dissolved, particulate and microbial components of a tidal saltmarsh-dominated estuary under contrasting levels of freshwater discharge, *Estuarine, Coastal and Shelf Science*, 2016, **182**, 72-85.

94. K. H. Altgelt and M. M. Boduszynski, *Composition and Analysis of Heavy Petroleum Fractions*, 1st edn., Marcel Dekker, Inc. New York 1994.

95. S. Kim, R. W. Kramer and P. G. Hatcher, Graphical Method for Analysis of Ultrahigh-Resolution Broadband Mass Spectra of Natural Organic Matter, the Van Krevelen Diagram, *Analytical Chemistry*, 2003, **75**, 5336-5344.

96. A. V. Callaghan, Metabolomic investigations of anaerobic hydrocarbon-impacted environments, *Curr Opin Biotechnol*, 2013, **24**, 506-515.

97. N. Das and P. Chandran, Microbial degradation of petroleum hydrocarbon contaminants: an overview, *Biotechnol Res Int*, 2011, **2011**, 941810.

98. G. Fuchs, M. Boll and J. Heider, Microbial degradation of aromatic compounds — from one strategy to four, *Nature Reviews Microbiology*, 2011, **9**, 803-816.

99. J. Heider, Adding handles to unhandy substrates: anaerobic hydrocarbon activation mechanisms, *Current Opinion in Chemical Biology*, 2007, **11**, 188-194.

100. L. K. Oberding and L. M. Gieg, Methanogenic Paraffin Biodegradation: Alkylsuccinate Synthase Gene Quantification and Dicarboxylic Acid Production, *Applied and Environmental Microbiology*, 2018, **84**, e01773-01717.

101. C. R. A. Toth and L. M. Gieg, Time Course-Dependent Methanogenic Crude Oil Biodegradation: Dynamics of Fumarate Addition Metabolites, Biodegradative Genes, and Microbial Community Composition, *Frontiers in Microbiology*, 2018, **8**.

102. H. P. Bacosa, D. L. Erdner and Z. Liu, Differentiating the roles of photooxidation and biodegradation in the weathering of Light Louisiana Sweet crude oil in surface water from the Deepwater Horizon site, *Marine Pollution Bulletin*, 2015, **95**, 265-272.

103. S. Bobinger and J. T. Andersson, Photooxidation Products of Polycyclic Aromatic Compounds Containing Sulfur, *Environmental Science & Technology*, 2009, **43**, 8119-8125.

104. P. Campo, A. D. Venosa and M. T. Suidan, Biodegradability of Corexit 9500 and Dispersed South Louisiana Crude Oil at 5 and 25 °C, *Environmental Science & Technology*, 2013, **47**, 1960-1967.

105. T. K. Dutta and S. Harayama, Fate of Crude Oil by the Combination of Photooxidation and Biodegradation, *Environmental Science & Technology*, 2000, **34**, 1500-1505.

106. R. M. Garrett, I. J. Pickering, C. E. Haith and R. C. Prince, Photooxidation of Crude Oils, *Environmental Science & Technology*, 1998, **32**, 3719-3723.

107. S. M. King, P. A. Leaf, A. C. Olson, P. Zito and M. A. Tarr, Photolytic and photocatalytic degradation of surface oil from the Deepwater Horizon spill, *Chemosphere*, 2014, **95**, 415-422.

108. R. C. Prince, R. M. Garrett, R. E. Bare, M. J. Grossman, T. Townsend, J. M. Suflita, K. Lee, E. H. Owens, G. A. Sergy, J. F. Braddock, J. E. Lindstrom and R. R. Lessard, The Roles of Photooxidation and Biodegradation in Long-term Weathering of Crude and Heavy Fuel Oils, *Spill Science & Technology Bulletin*, 2003, **8**, 145-156.

109. M. Seidel, S. Kleindienst, T. Dittmar, S. B. Joye and P. M. Medeiros, Biodegradation of crude oil and dispersants in deep seawater from the Gulf of Mexico: Insights from ultra-high resolution mass spectrometry, *Deep Sea Research Part II: Topical Studies in Oceanography*, 2016, **129**, 108-118.

110. L. St. Mary, L. S. D. Trine, C. Roper, J. Wiley, S. L. Massey Simonich, M. McCoustra and T. B. Henry, Time-Related Alteration of Aqueous-Phase Anthracene and Phenanthrene Photoproducts in the Presence of TiO2 Nanoparticles, *Environmental Science & Technology*, 2021, **55**, 3727-3735.

111. H. Yu, Environmental Carcinogenic Polycyclic Aromatic Hydrocarbons: Photochemistry and Phototoxicity, *Journal of Environmental Science and Health, Part C*, 2002, **20**, 149-183.

112. B. A. Bekins, J. C. Brennan, D. E. Tillitt, I. M. Cozzarelli, J. M. Illig and D. Martinović-Weigelt, Biological Effects of Hydrocarbon Degradation Intermediates: Is the Total Petroleum Hydrocarbon Analytical Method Adequate for Risk Assessment?, *Environmental Science & Technology*, 2020, **54**, 11396-11404.

APPENDICES

Appendix A1: Instrumentation Parameters

LC-Orbitrap Instrument Parameters

SPE- DOC extracts were analyzed using a Vanquish Flex Binary ultra-high performance liquid chromatograph coupled to an Exploris 120 high resolution orbitrap mass spectrometer (Thermo Scientific). Samples were injected (20 µL) onto a Kinetix C18 column (150 x 2.1mm; 1.7µ) with an Ultra-high pressure liquid chromatography (UHPLC) C18 2.1 mm Security Guard Column (Phenomenex) and eluted at 0.4 mL min^{-1} using with a gradient of water (A) and acetonitrile (B) each containing 0.1% formic acid (v/v). The column was maintained at 60 °C while the mobile phase composition was ramped from 5 to 99% B over 15 min and held for 10 min before resetting to initial conditions; total run time was 32 min. Eluted compounds were ionized via negative mode electrospray ionization (3200V). The nitrogen sheath gas, auxiliary gas, and sweep gas flows were 50, 5, and 5 (arbitrary units), respectively. The vaporizer and ion transfer tube temperatures were 350 and 300 °C. Ionization parameters were optimized by infusing the calibration solution (FlexMix, Thermo Scientific) into 0.4 mL/min 50% A post column at 5 µL/min. Full scans were collected over the range 150-1500 *m/z* with a resolution of 120,000 and RF lens set to 70%. Automatic gain control was used to accumulate 1e6 ions in the trap allowing a maximum injection time of 200 ms. Orbitrap mass accuracy was externally calibrated prior to analysis via infusion of the calibration solution while a mass lock was established during each scan using the fluoranthene (M^-, 202.0788 *m/z*) internal calibrant discharge source (Easy-IC, Thermo Scientific). A standard solution containing 10 µg/mL each of metsulfuron methyl, chlorsulfuron, capsaicin, rotenone, usnic acid, and ibuprofen was analyzed after every ten samples for quality assurance.

Targeted oxyPAH and PAH Instrument Parameters

OxyPAHs and PAHs were analyzed separately using a 1260 Infinity series liquid chromatograph coupled to a 6410A triple quadrupole mass spectrometer controlled by Mass Hunter v. B.06.00 (Agilent). 10 µL injections were made onto a Zorbax Eclipse PAH (2.1x100 mm; 3.5µm) column with matching guard cartridge (2.1x12.5 mm; 5µ) (Agilent) and eluted at 0.2 mL min^{-1} with a gradient of water (A) and methanol (B) each containing 0.1% formic acid, the column compartment was maintained at 40 °C. Gradient parameters for OxyPAHs and PAHs are available in the supporting information (**Table A8 and A9**). OxyPAHs were ionized via negative mode atmospheric pressure photoionization (APPI) assisted with post column addition of acetone (0.4 mL min^{-1} of 85:15 methanol:acetone v/v; final composition 10% acetone) dopant. PAHs were ionized via postive mode APPI assisted with post column addition of chlorobenzene and 2,4-difluoroanisole (0.4 mL min^{-1} of 84.25:15:0.75 methanol:chlorobenzene:2,4-difluoroanisole v/v; final composition 10% chlorobenzene and 0.5% 2,4-difluoroanisole) dopant. Analyte retention times and triple quadrupole acquisition parameters are available in the supporting information (**Table A10**).

Appendix Table A1. DOC and $SUVA_{254}$ values. (Averages N=3)

Sample Composition			DOC (mg/L)		SUVA254 (L mg-1 cm-1)	
Fuel	**Light Type**	**Irradiation Period (days)**	**Average**	**Standard Deviation**	**Average**	**Standard Deviation**
Cook Inlet Crude Oil	Light	1	4.22	2.764	0.01	0.005
		4	10.61	2.028	0.015	0.002
		7	18.84	4.931	0.0168	0.004
		10	20.54	2.319	0.0169	0.001
	Dark	1	0.84	0.067	0.008	0.002
		4	1.59	0.408	0.0029	0.001
		7	1.67	0.158	0.0024	0
		10	1.47	0.291	0.0034	0.002
Diesel	Light	1	6.27	0.521	0.0108	0.001
		4	11.51	0.885	0.0139	0.001
		7	13.49	1.294	0.0137	0.003
		10	14.76	0.993	0.0128	0
	Dark	1	0.77	0.209	0.0056	0.002
		4	1.05	0.338	0.0058	0.005
		7	0.98	0.179	0.0045	0.001
		10	0.95	0.124	0.0046	0

Appendix Table A2.a. Spectral Indices (Raman Specific Units, RSU). (Averages N=3)

Sample Composition			T		A		M		C		N	
Fuel	**Light Type**	**Irradiation Period (days)**	**Average**	**Standard Deviation**	**Average**	**Standard Deviation**	**Average**	**Standard Deviation**	**Average**	**Standard Deviation**	**Average**	**Standard Deviation**
Cook Inlet Crude Oil	Light	1	1.71	0.36	1.69	0.5	1.34	0.35	0.43	0.11	1.42	0.37
		4	2.84	0.19	4.07	0.25	3.22	0.18	1.27	0.56	3.35	0.18
		7	1.68	0.34	2.42	0.28	2.05	0.3	0.62	0.06	2.12	0.31
		10	1.16	0.28	1.5	0.3	1.33	0.29	0.42	0.1	1.39	0.29
	Dark	1	0.14	0.04	0.05	0.01	0.05	0.01	0.02	0	0.06	0.02
		4	0.24	0.15	0.07	0.02	0.09	0.04	0.02	0.01	0.1	0.05
		7	0.14	0	0.06	0	0.06	0	0.02	0	0.07	0.01
		10	0.13	0.02	0.07	0.01	0.06	0.01	0.02	0	0.06	0.01
Diesel	Light	1	4.99	0.22	0.66	0.07	1.4	0.07	0.26	0.03	1.43	0.08
		4	2.5	0.28	0.52	0.03	0.79	0.08	0.24	0.01	0.84	0.08
		7	1.3	0.16	0.34	0.07	0.47	0.08	0.17	0.03	0.49	0.09
		10	0.9	0.11	0.25	0.04	0.34	0.05	0.12	0.02	0.36	0.05
	Dark	1	0.08	0.02	0.06	0.04	0.03	0.01	0.02	0.01	0.03	0.01
		4	0.08	0.02	0.04	0.02	0.02	0.01	0.01	0	0.03	0.01
		7	0.09	0.02	0.04	0.02	0.03	0.01	0.01	0	0.03	0.01
		10	0.04	0.04	0.02	0.01	0.01	0.01	0.01	0	0.01	0.01

Appendix Table A2.b. Spectral Indices (Raman Specific Units, RSU). (Averages N=3)

Sample Composition			FluI		FrI		BIX		HIX	
Fuel	**Light Type**	**Irradiation Period (days)**	**Average**	**Standard Deviation**	**Average**	**Standard Deviation**	**Average**	**Standard Deviation**	**Average**	**Standard Deviation**
Cook Inlet Crude Oil	Light	1	1.21	0.02	1.44	0.02	1.63	0.03	0.58	0.03
		4	1.22	0.01	1.31	0.02	1.43	0.03	0.68	0
		7	1.2	0.02	1.22	0.03	1.29	0.04	0.69	0.01
		10	1.18	0.01	1.15	0.04	1.21	0.05	0.66	0.01
	Dark	1	1.4	0.03	1.57	0.04	1.69	0.05	0.28	0.03
		4	1.45	0.06	1.62	0.19	1.76	0.17	0.29	0.07
		7	1.4	0.06	1.69	0.04	1.89	0.07	0.31	0.01
		10	1.35	0.04	1.69	0.05	1.91	0.13	0.35	0.04
Diesel	Light	1	1.19	0.02	1.35	0.04	1.37	0.03	0.36	0.02
		4	1.19	0.01	0.89	0.01	0.9	0.01	0.3	0.02
		7	1.19	0.02	0.82	0.05	0.82	0.04	0.24	0.05
		10	1.14	0.02	0.81	0.01	0.83	0.02	0.2	0.01
	Dark	1	1.48	0.07	1.34	0.35	1.48	0.35	0.3	0.03
		4	1.35	0.06	1.39	0.2	1.58	0.25	0.24	0.07
		7	1.41	0.06	1.56	0.16	1.72	0.09	0.23	0.06
		10	1.4	0.08	1.14	0.36	1.28	0.29	0.34	0.11

Appendix Table A3.a. Relative contribution of PARAFAC components (%). (Averages N=3)

Sample Composition			C1		C2		C3	
Fuel	**Light Type**	**Irradiation Period (days)**	**Average**	**Standard Deviation**	**Average**	**Standard Deviation**	**Average**	**Standard Deviation**
Cook Inlet Crude Oil	Light	1	42.03	0.89	23.03	1.18	5.03	0.38
		4	48.15	0.16	25.29	0.75	4.51	0.1
		7	49.32	0.49	23.31	0.39	5.1	0.33
		10	48.38	0.46	20.19	0.71	6.85	0.37
	Dark	1	19.56	1.93	10.28	1.98	36.25	6.85
		4	19.36	2.64	10.37	4.2	28.29	7.88
		7	21.62	1.39	12.98	1.24	29.9	5.01
		10	27.03	5.11	11.93	1.57	24.52	1.74
Diesel	Light	1	17.3	0.41	1.42	0.06	33.83	1.06
		4	14.97	0.68	1.28	0.11	52.96	1.68
		7	13.5	3.23	1.61	0.53	56.35	5.15
		10	11.01	1.03	1.64	0.2	58.86	1.84
	Dark	1	22.6	4.31	4.51	0.14	40.36	1.98
		4	18.17	4.66	5.11	0.53	36.06	4.35
		7	19.28	8.19	5.34	0.97	33.78	5.47
		10	19.45	4.92	1.72	2.98	48.72	9.66

Appendix Table A3.b. Relative contribution of PARAFAC components (%). (Averages N=3)

Sample Composition			C4		C5		C6	
Fuel	**Light Type**	**Irradiation Period (days)**	**Average**	**Standard Deviation**	**Average**	**Standard Deviation**	**Average**	**Standard Deviation**
Cook Inlet Crude Oil	Light	1	16.87	1.27	9.52	0.36	3.52	0.53
		4	9.77	0.22	9.95	0.77	2.33	0.17
		7	7.7	1.12	10.52	0.83	4.06	0.23
		10	6.9	0.27	11.02	0.64	6.66	0.19
	Dark	1	18.68	2.19	6.22	0.45	9.01	9.06
		4	20.16	1.72	5.81	0.83	16.02	14.64
		7	18.48	2.98	5.73	0.71	11.29	7.33
		10	14.25	3.44	6.91	1.06	15.36	2.92
Diesel	Light	1	39.44	1.01	6.29	0.38	1.72	0.23
		4	15.2	0.48	5.45	0.44	10.13	0.3
		7	7.6	2.55	5.06	1.02	15.86	2.17
		10	3.39	0.71	4.15	0.39	20.96	0.95
	Dark	1	6.67	1.76	9.46	2.49	16.4	1.81
		4	9.66	2.24	8	1.56	23	4.94
		7	12.64	6.74	7.26	1	21.71	4.19
		10	10.37	3.7	8.68	2.42	11.07	11.06

Appendix Figure A1. Validated six-component PARAFAC model.

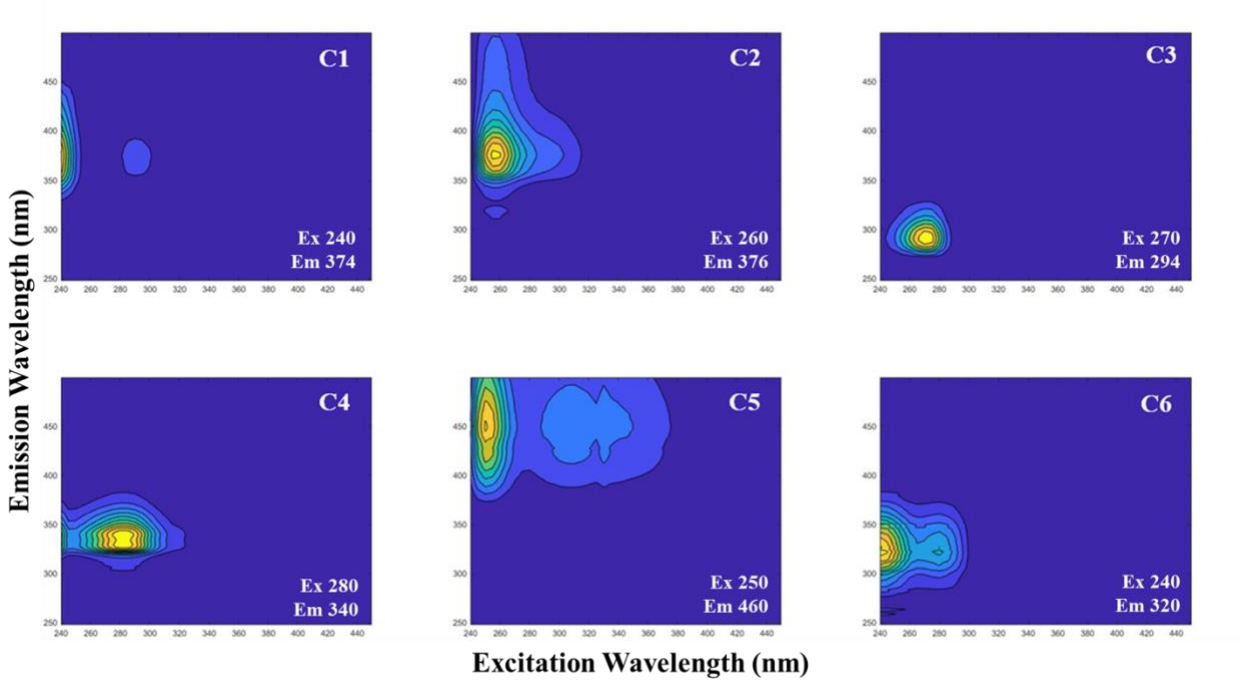

Appendix Table A4.a. Molecular classifications of unique features in each treatment group. (Averages N=3)

Sample Composition			Unique Features (#)	CA (%)		Aromatic (%)		ULO (%)	
Fuel	**Light Type**	**Irradiation Period (days)**		**Average**	**Standard Deviation**	**Average**	**Standard Deviation**	**Average**	**Standard Deviation**
Cook Inlet Crude Oil	Light	4	2483	3.63	0.47	15.94	2.17	54.31	4.37
		7	2492	3.08	0.76	11.9	4.3	48.01	15.1
		10	2484	3.25	0.29	12.22	0.41	52.77	5.58
	Dark	10	1010	3.08	0.95	7.94	3.13	15.17	1.83
Diesel	Light	4	1986	1.12	0.21	12.94	1.7	65.14	4.95
		7	2090	0.97	0.66	10.39	0.76	60.93	13.81
		10	2293	0.67	0.05	9.93	0.49	64.69	4.07
	Dark	10	1722	2.07	0.15	2.82	1	16.3	1.55

Appendix Table A4.b. Molecular classifications of unique features in each treatment group. (Averages N=3)

Sample Composition			Unique Features (#)	UHO (%)		Aliphatic (%)	
Fuel	**Light Type**	**Irradiation Period (days)**		**Average**	**Standard Deviation**	**Average**	**Standard Deviation**
Cook Inlet Crude Oil	Light	4	2483	1.33	0.33	24.73	7.24
		7	2492	1.75	0.4	35.26	20.38
		10	2484	3.54	0.88	28.25	5.9
	Dark	10	1010	16.33	7.13	57.48	6.34
Diesel	Light	4	1986	1.57	0.46	19.21	6.24
		7	2090	1.86	0.42	25.94	12.64
		10	2293	2.42	0.17	22.33	4.81
	Dark	10	1722	26.85	5.48	51.96	4.69

Appendix Table A5.a. Molecular classification (%), averages masses, and NOSC. (Averages N=3)

Sample Composition			CA		Aromatic		ULO		UHO	
Fuel	**Light Type**	**Irradiation Period (days)**	**Average**	**Standard Deviation**	**Average**	**Standard Deviation**	**Average**	**Standard Deviation**	**Average**	**Standard Deviation**
Cook Inlet Crude Oil	Light	4	4.89	0.17	11.32	0.37	46.63	3.95	6.65	0.35
		7	4.31	0.82	10.79	0.92	47.23	2.05	6.9	0.87
		10	4.23	0.7	10.6	0.7	46.47	1.79	8.81	0.77
	Dark	10	2.93	0.1	6.03	0.91	30.11	0.94	19.18	1.48
Diesel	Light	4	3.07	0.3	9.46	0.96	46.73	1.22	7	1.04
		7	2.98	0.86	8.8	1.24	48.53	0.61	6.63	0.97
		10	2.56	0.13	8.15	0.08	48.61	2.05	7.06	0.24
	Dark	10	2.46	0.22	4.38	0.34	24.17	0.43	21.21	2.03

Appendix Table A5.b. Molecular classification (%), averages masses, and NOSC. (Averages N=3)

Sample Composition			Aliphatic		Naphthenic Acids		NOSC		Average Mass	
Fuel	**Light Type**	**Irradiation Period (days)**	**Average**	**Standard Deviation**	**Average**	**Standard Deviation**	**Average**	**Standard Deviation**	**Average**	**Standard Deviation**
Cook Inlet Crude Oil	Light	4	28.72	3.99	1.79	0.17	-0.75	0.06	395.26	8.96
		7	28.83	1.98	1.93	0.38	-0.78	0.06	407.46	23
		10	28.1	1.33	1.78	0.35	-0.72	0.04	426.22	10.97
	Dark	10	39.8	0.75	1.95	0.1	-0.66	0.07	329.85	3.95
Diesel	Light	4	31.77	3.3	1.96	0.1	-0.71	0.04	403.07	6.68
		7	31.18	2.74	1.88	0.16	-0.72	0	413.17	20.49
		10	31.68	1.98	1.93	0.16	-0.73	0.01	436.11	9.35
	Dark	10	46.11	1.81	1.66	0.13	-0.63	0.07	341.66	7.96

Appendix Table A6.a. PAH and oxyPAH concentrations.

Sample Composition			Oxy-PAH			
			Phenanthrequinone		1,4-Anthraquinone	
Fuel	Light Type	Irradiation Period (days)	Average	Standard Deviation	Average	Standard Deviation
Cook Inlet Crude Oil	Light	1	ND	--	ND	--
		4	ND	--	0.14	0.12
		7	0.11	0.1	0.21	0.01
		10	0.13	0.11	0.19	0.16
Diesel	Light	1	ND	--	ND	--
		4	ND	--	ND	--
		7	ND	--	ND	--
		10	ND	--	ND	--

Appendix Table A6.b. PAH and oxyPAH concentrations.

Sample Composition			PAH			
			Naphthalene		1-Methylnaphthalene	
Fuel	Light Type	Irradiation Period (days)	Average	Standard Deviation	Average	Standard Deviation
Cook Inlet Crude Oil	Light	1	2.42	2.28	17.12	4.76
		4	0.36	0.32	7.39	4.86
		7	ND	--	1.07	0.51
		10	ND	--	0.33	0.33
Diesel	Light	1	15.49	19.01	60.44	62.49
		4	8.58	0.97	0.18	0.16
		7	28.62	44.45	0.14	0.23
		10	4.17	1.56	0.09	0.16

Appendix Table A6.c. PAH and oxyPAH concentrations.

Sample Composition			PAH					
			2-Methylnaphthalene		Acenaphthene		Fluorene	
Fuel	Light Type	Irradiation Period (days)	Average	Standard Deviation	Average	Standard Deviation	Average	Standard Deviation
Cook Inlet Crude Oil	Light	1	16.14	4.58	ND	--	0.8	0.03
		4	6.74	4.57	ND	--	0.45	0.09
		7	1.24	0.33	ND	--	0.18	0.16
		10	0.61	0.22	ND	--	0.97	0.04
Diesel	Light	1	125.15	136.23	1.96	1.26	1.56	0.97
		4	0.7	0.12	0.06	0.11	0.54	0.27
		7	0.4	0.1	ND	--	ND	--
		10	0.33	0.04	ND	--	ND	--

Appendix Table A6.d. PAH and oxyPAH concentrations.

Sample Composition			PAH					
			Phenanthrene		2,6-Dimethylnaphthalene		Anthracene	
Fuel	Light Type	Irradiation Period (days)	Average	Standard Deviation	Average	Standard Deviation	Average	Standard Deviation
Cook Inlet Crude Oil	Light	1	1.5	0.09	0.7	0.24	0.1	0.18
		4	1.73	0.14	0.54	0.29	0	0
		7	1.41	0.03	ND	--	0.23	0.4
		10	1.02	0.31	ND	--	0	0
Diesel	Light	1	0.75	0.41	15.17	11.73	ND	--
		4	0.31	0.18	0.5	0.31	ND	--
		7	0.09	0.08	ND	--	ND	--
		10	0	0	ND	--	ND	--

Appendix Table A6.e. PAH and oxyPAH concentrations.

Sample Composition			2,3,6-Trimethylnaphthalene		Pyrene		1-Methylpyrene	
Fuel	**Light Type**	**Irradiation Period (days)**	**Average**	**Standard Deviation**	**Average**	**Standard Deviation**	**Average**	**Standard Deviation**
Cook Inlet Crude Oil	Light	1	0.31	0.15	0.08	0.01	0.28	0.04
		4	0.09	0.15	0.08	0.02	0.25	0
		7	ND	--	0.11	0.05	0.23	0.02
		10	ND	--	ND	--	ND	--
Diesel	Light	1	12.7	6.86	0.07	0.07	ND	--
		4	0.91	0.62	0.04	0.06	0.08	0.13
		7	ND	--	ND	--	0.06	0.11
		10	ND	--	0.04	0.07	0	0

Appendix Table A7. Retention time, recoveries, and instrument parameters for oxyPAH method.

Name	Transition	Type	RT (min)	Recovery (%) (N=6)	
				Average	**Standard Deviation**
1-Naphthol	143.1 -> 115.1	Target	19.8	73.8	12.4
2-Naphthol	143.1 -> 115.1	Target	20.6	72.5	12.2
Phenanthrenequinone	208.1 -> 208.1	Target	22.3	69.3	13.6
Anthraquinone	208.1 -> 208.1	Target	26.9	24.8	7.7
1,4-Anthraquinone	208.1 -> 208.1	Target	30.4	79.5	13.7
1-Hydroxy-9,10-Anthraquinone	224.1 -> 224.1	Target	35.6	79.2	14.9
1,4-Chrysenequinone	258.1 -> 258.1	Target	46	5.8	1.8
5,12-Naphthacenequinone	258.1 -> 258.1	Target	47.4	88.4	15.2
Benzanthraquinone	258.1 -> 258.1	Target	50.8	81.9	16.5

Appendix Table A8. oxyPAH gradient parameters.

Pump 1 (Column Mobile Phase)					Pump 2 (Post Column Ionization Additives)				
Time (min)	**A (%)**	**B (%)**	**Flow (mL/min)**	**Max Pressure Limit (bar)**	**Time (min)**	**A (%)**	**B (%)**	**Flow (mL/min)**	**Max Pressure Limit (bar)**
0	40	60	0.2	400	**0**	0	100	0	400
1	40	60	0.2	400	**9.99**	0	100	0	400
5	60	40	0.2	400	**10**	0	100	0.4	400
65	100	0	0.2	400	**70**	0	100	0.4	400
70	100	0	0.2	400	**70.1**	0	100	0.4	400
70.1	40	60	0.4	400					

Appendix Table A9. PAH gradient parameters.

	Pump 1 (Column Mobile Phase)				Pump 2 (Post Column Ionization Additives)				
Time (min)	**A (%)**	**B (%)**	**Flow (mL/min)**	**Max Pressure Limit (bar)**	**Time (min)**	**A (%)**	**B (%)**	**Flow (mL/min)**	**Max Pressure Limit (bar)**
0	20	80	0.2	400	**0**	100	0	0	400
1	20	80	0.2	400	**18.99**	100	0	0	400
20	60	40	0.2	400	**19**	100	0	0.4	400
33	71	29	0.2	400	**59.99**	100	0	0.4	400
36	75	25	0.2	400	**60**	100	0	0	400
46	75	25	0.2	400					
56	90	10	0.2	400					
60	90	10	0.2	400					
60.01	20	80	0.4	400					
65	20	80	0.4	400					
65.01	20	80	0.2	400					

Appendix Table A10.a. Retention time and instrument parameters for PAH method

Compound Name	Transition	Type	ISTD Compound Name	Surrogate Compound Name	RT (min)	Recovery (%) (N=6)	
						Average	Standard Deviation
Naphthalene d8	136.0 -> 108.0	Surrogate	Acenapthylene d8		15.8		
Naphthalene	128.0 -> 102.0	Target	Acenapthylene d8	Napthalene d8	16.2		
Acenapthylene d8	160.0 -> 132.0	ISTD			18		
Acenaphthylene	152.0 -> 126.0	Target	Acenapthylene d8	Napthalene d8	18.5		
1-Methyl Naphthalene d10	152.0 -> 122.0	ISTD			19.9		
1-Methyl Naphthalene	142.0 -> 115.0	Target	1-Methyl Naphthalene d10	Acenapthene d10	20.5	96.3	7.8
2-Methyl Naphthalene	142.0 -> 115.0	Target	1-Methyl Naphthalene d10	Acenapthene d10	21.2	125.4	26
Acenaphthene d10	164.0 -> 162.0	Surrogate	1-Methyl Naphthalene d10		22.1		
Acenaphthene	154.0 -> 153.0	Target	1-Methyl Naphthalene d10	Acenapthene d10	22.7	100.5	5
Fluorene d10	176.0 -> 174.0	ISTD			24		
Fluorene	166.0 -> 165.0	Target	Fluorene d10	Phenanthrene d10	24.6	95.8	4.8
Phenanthrene d10	188.0 -> 184.0	Surrogate	Fluorene d10		26		
9-methyl-9H-fluorene	180.1 -> 165.2	Target	Fluorene d10	Phenanthrene d10	26.6	89.7	6.9
Phenanthrene	178.0 -> 176.0	Target	Fluorene d10	Phenanthrene d10	27	97.3	14.9
2,6-Dimethylnaphthalene	156.0 -> 115.0	Target	Fluorene d10	Phenanthrene d10	28.2		
Anthracene	178.0 -> 176.0	Target	Fluorene d10	Phenanthrene d10	30	94.2	5.3
Fluoranthene	202.0 -> 200.0	Target	Chrysene d12	Pyrene d10	33.1		
2,3,6-Trimethylnaphthalene	170.2 -> 155.1	Target	Chrysene d12	Pyrene d10	33.4		
Pyrene d10	212.0 -> 208.0	Surrogate	Chrysene d12		33.9		
9-methylanthracene	192.2 -> 191.1	Target	Chrysene d12	Pyrene d10	34.2	89.8	3.3

Appendix Table A10.b. Retention time and instrument parameters for PAH method

Compound Name	Transition	Type	ISTD Compound Name	Surrogate Compound Name	RT (min)	Recovery (%) (N=6)	
						Average	Standard Deviation
Pyrene	202.0 -> 200.0	Target	Chrysene d12	Pyrene d10	34.9	115.7	10.5
9,10-Dimethylanthracene	206.2 -> 191.1	Target	Chrysene d12	Benz(a)anthracene d10	38.8		
1-Methylpyrene	216.2 -> 215.2	Target	Chrysene d12	Benz(a)anthracene d10	42.3		
Benz(a)anthracene d10	240.0 -> 236.0	Surrogate	Chrysene d12		43.3		
Benz(a)anthracene	228.0 -> 226.0	Target	Chrysene d12	Benz(a)anthracene d10	44.5	95.5	5
Chrysene d12	240.0 -> 236.0	ISTD			44.9		
Chrysene	228.0 -> 226.0	Target	Chrysene d12	Benz(a)anthracene d10	46.3	99.3	6
Perylene d12	264.0 -> 260.0	Surrogate	Chrysene d12		50.1		
Benzo(a)pyrene	252.0 -> 250.0	Target	Benzo(a)pyrene d12	Perylene d12	52		
Benzo(a)pyrene d12	264.0 -> 260.0	ISTD			55.1		
Benzo(b)fluoranthene	252.0 -> 250.0	Target	Benzo(a)pyrene d12	Perylene d12	56.3	96.2	3
Benzo(k)fluoranthene	252.0 -> 250.0	Target	Benzo(a)pyrene d12	Perylene d12	56.4	96.7	4.6
Benzo(ghi)perylene	276.0 -> 274.0	Target	Benzo(a)pyrene d12	Perylene d12	61.3	93.7	5.8
Dibenzo(ah)anthracene	278.0 -> 276.0	Target	Benzo(a)pyrene d12	Perylene d12	64	96.1	7.9
Indenopyrene	276.0 -> 274.0	Target	Benzo(a)pyrene d12	Perylene d12	64.2	96.2	7

U.S. Department of the Interior (DOI)
The DOI protects and manages the Nation's natural resources and cultural heritage; provides scientific and other information about those resources; and honors the Nation's trust responsibilities or special commitments to American Indians, Alaska Natives, and affiliated island communities.

Bureau of Ocean Energy Management (BOEM)
BOEM's mission is to manage development of U.S. Outer Continental Shelf energy and mineral resources in an environmentally and economically responsible way.

BOEM Environmental Studies Program
The mission of the Environmental Studies Program is to provide the information needed to predict, assess, and manage impacts from offshore energy and marine mineral exploration, development, and production activities on human, marine, and coastal environments. The proposal, selection, research, review, collaboration, production, and dissemination of each of BOEM's Environmental Studies follows the DOI Code of Scientific and Scholarly Conduct, in support of a culture of scientific and professional integrity, as set out in the DOI Departmental Manual (305 DM 3).